Elsevier Editorial System(tm) for Journal of Marine Systems
Manuscript Draft

Manuscript Number: MARSYS-D-12-00119

Title: Connecting Atlantic Temperature Variability and Biological Cycling in two Earth System Models

Article Type: Special Issue: AMO Impact

Keywords: Atlantic meridional overturning; primary productivity; decadal variability; earth system modelling

Corresponding Author: Dr. Anand Gnanadesikan,

Corresponding Author's Institution: Johns Hopkins University

First Author: Anand Gnanadesikan

Order of Authors: Anand Gnanadesikan; John Dunne, Ph.D.; Rym Msadek, Ph.D.

Abstract: A connection between the interdecadal variability in North Atlantic temperatures and biological cycling has been widely hypothesized, but the exact mechanism driving such connections remains obscure. We examine the interdecadal variability in the annual and month-by-month diatom biomass in two Earth System Models run at the Geophysical Fluid Dynamics Laboratory. The models have the same formulations of atmospheric, land, sea ice and ocean biogeochemical dynamics but different formulations of ocean physics. One of these models (ESM2M) uses the traditional level-coordinate formulation for ocean physics while the other (ESM2G) uses a newer formulation based on isopycnal layers. The two models show quite different connections between Atlantic temperatures and biological cycling. ESM2G exhibits realistically low levels of summertime nutrients in the North Atlantic so that the biology in key regions is sensitive to the depth of wintertime convection and/or the location of nutrient fronts. In ESM2G both these biologically important phenomena and Atlantic temperatures are strongly correlated with the meridional overturning circulation. By contrast, ESM2M has much higher levels of nutrients throughout the subpolar gyre, so that biological variability depends much more on light limitation. Although some signature of variability is found in the spring, in general ESM2M has much lower interannual variability than ESM2G and little of it is related to the mean Atlantic temperature.

Highlights

We relate the AMO index to variability in diatom biomass.

Both biomass and AMO index can be consequences of changes in overturning.

Nutrient supply changes drive changes off West Greenland and the Bay of Biscay.

Light supply associated with ice meltback drives changes of the Labrador Coast.

Results may explain interdecadal changes in Greenland cod stocks.

Olin 327
Johns Hopkins University
3400 N. Charles St.
Baltimore, MD 21218
May 16, 2012

Prof. Juergen Alheit
Guest Editor, Journal of Marine Systems

Dear Juergen,

I'm happy to offer the attached manuscript "Connecting Atlantic Temperature Variability and Biological Cycling in two Earth System Models" for inclusion in the Special Issue arising from the AMO Workshop. Thank you for including me in this process- I have learned a lot! And my sincere apologies for the delays in submitting this paper.

Best,
Anand Gnanadesikan
Assoc. Prof.
Dept. of Earth and Planetary Sciences

Connecting Atlantic Temperature Variability and Biological Cycling in two Earth System Models

Anand Gnanadesikan
Johns Hopkins University, Baltimore, MD USA
gnanades@jhu.edu

John P. Dunne and Rym Msadek
Geophysical Fluid Dynamics Laboratory, Princeton, NJ USA
john.dunne@noaa.gov, rym.msadek@noaa.gov

Abstract

A connection between the interdecadal variability in North Atlantic temperatures and biological cycling has been widely hypothesized, but the exact mechanism driving such connections remains obscure. We examine the interdecadal variability in the annual and month-by-month diatom biomass in two Earth System Models run at the Geophysical Fluid Dynamics Laboratory. The models have the same formulations of atmospheric, land, sea ice and ocean biogeochemical dynamics but different formulations of ocean physics. One of these models (ESM2M) uses the traditional level-coordinate formulation for ocean physics while the other (ESM2G) uses a newer formulation based on isopycnal layers. The two models show quite different connections between Atlantic temperatures and biological cycling. ESM2G exhibits realistically low levels of summertime nutrients in the North Atlantic so that the biology in key regions is sensitive to the depth of wintertime convection and/or the location of nutrient fronts. In ESM2G both these biologically important phenomena and Atlantic temperatures are strongly correlated with the meridional overturning circulation. By contrast, ESM2M has much higher levels of nutrients throughout the subpolar gyre, so that biological variability depends much more on light limitation. Although some signature of variability is found in the spring, in general ESM2M has much lower interannual variability than ESM2G and little of it is related to the mean Atlantic temperature.

Introduction

Changes in the mean sea surface temperature of the Atlantic have been associated with climate shifts around the northern hemisphere (Schlesinger and Ramankutty, 1994), and are sometimes referred to as the Atlantic Multidecadal Oscillation (AMO). Enfield et al., (2001) proposed an AMO index, corresponding to the decadally-smoothed mean temperature of the Atlantic between the equator and 70N, and showed that this index is correlated with rainfall over the Mississippi basin and Southern Florida. Locally, changes in ocean temperature have also been linked to ecosystem shifts, including changes in the cod fishery off of Greenland (Jensen, 1939; Stein, 2007) and Norway (Sundby and Nakken, 2008) and changes in species composition in a number of locations (Collie et al., 2008 in Narragansett Bay; Dulvy et al, 2008 in the North Sea; Nye et al. 2009, in the mid-Atlantic bight). The ICES/PICES workshop on the AMO leading to this special issue was convened in part to evaluate whether these changes could be linked to the AMO index, and whether such linkage might provide some level of predictability. The relatively short record of Atlantic temperatures makes it unclear whether the AMO is truly an oscillation or simply reflects red-noise variability. In order to sidestep this question we will consider whether the AMO index is a useful measure of the state of the Atlantic.

It is far from clear that local changes in SST and ecosystems should be directly related to the relatively small changes in basin-averaged SST associated with the AMO index. While possible mechanisms invoked in, for example Nye et al. 2009, include changes in the optimal temperature range for various species, the AMO index is

57 associated with O(0.1-0.2°C) changes in the basin-mean decadal temperature (Sutton and
58 Hodson, 2005). Given that north-south temperature gradients average ~0.3-0.4°C per
59 degree latitude, it is hard to see that such small changes should produce first-order effects
60 on ecosystems.

61 However, it is also likely that the AMO index is a proxy for other changes more
62 directly relevant to biological cycling. In numerical models, the AMO index is closely
63 related to the Atlantic Meridional Overturning Circulation, (Delworth and Mann, 2000).
64 This means that changes in the AMO index may be the result of large-scale
65 reorganizations of the circulation which both change the transport of heat into the basin
66 and the release of that heat to the atmosphere. Additionally, when Zhang and Delworth
67 (2006) modeled the impact of such changes in meridional ocean heat transport on climate
68 they found interdecadal changes in rainfall over Africa and India and changes in vertical
69 wind shear sufficient to alter tropical cyclone activity over the Atlantic. Such indirect
70 impacts of changes in Atlantic SSTs may be important for various ecosystems.

71 In this paper, we focus on how decadal variability in primary production is linked
72 with decadal variability in mean Atlantic temperatures within two models that represent
73 the coupling between atmosphere, ocean, land, sea ice and ecosystems. These Earth
74 System Models, developed by the Geophysical Fluid Dynamics Laboratory, have
75 identical representation of atmosphere and both terrestrial and oceanic ecosystems, but
76 different representations of ocean physics. One of these models, denoted as ESM2M,
77 employs a vertical discretization in which the ocean volume is broken up into boxes
78 which represent ranges in pressure/depth. The other, denoted as ESM2G, uses an
79 isopycnal formulation in which the vertical discretization consists of variable-depth

layers which in the interior correspond to layers of constant density. Isopycnal models are able to resolve key physical aspects of the physics of the dense overflows that form an important part of the North Atlantic Overturning that are not well-represented in depth-coordinate models (Winton et al., 1998; Legg et al., 2006).

The representation of ocean biogeochemical cycling within these models includes an explicit representation of phytoplankton functional groups and associated biogeochemical cycling that make up the base of the marine food web. We use the models to examine the following questions

1. Is there a relationship between the AMO index and the variability in the magnitude or timing of phytoplankton blooms in the North Atlantic?
2. How different are these relationships across the basin?
3. How robust are these relationships to the formulation of ocean physics in the Earth System Model?

The structure of this paper is as follows. In the following section, we briefly sketch the important components of our physical and biogeochemical models. In Section 3, we examine the variability of the AMO index in the models, and examine its connection to the overturning circulation. In Section 4, we continue by looking at the connection between the AMO index and large diatom biomass, and show that this is very different between the two models. We examine how differences in the baseline biogeochemical simulation as well as differences in the drivers of temperature variability in the Atlantic in the two models result in these different behaviors.

2. Methods

a. Physical models

The atmospheric, land surface and sea ice components of the Earth System Model used in this paper originated from that used in the GFDL CM2.1 series (Delworth et al., 2006; Gnanadesikan et al., 2006) and are described in detail in Dunne et al. (2012). The atmospheric model has a resolution of 2x2.5 degrees and 24 vertical levels, with six of them in the lower boundary layer. Two ocean models are used. The first is the pressure-coordinate code MOM4.1 (Griffies, 2009; Dunne et al., 2012), with up-to-date parameterizations of mixed layer dynamics and mesoscale eddy mixing (Ferrari et al., 2010), and a new parameterization of submesoscale mixing (Fox-Kemper et al., 2011). Vertical diffusion in the deep ocean uses the Simmons et al. (2004) parameterization which links turbulent mixing coefficients to the rate of internal wave generation by the barotropic tides.

The second model is the Generalized Ocean Layer Dynamics (GOLD) code (Hallberg, 1995, Hallberg and Adcroft 2009, Dunne et al., 2012), configured as an isopycnal layer model in the ocean interior with a four layer surface layer. Earlier versions of this model are reported in Harrison and Hallberg (2008) and Gnanadesikan and Anderson (2009). Differences between previous versions of the GOLD model and the one used in this code include the implementation of the Simmons et al. (2004) deep tidal diffusion, implementation of a lower background diapycnal diffusion near the equator following Harrison and Hallberg (2008) and implementation of the mixed layer restratification of Fox-Kemper et al. (2011). A potentially significant difference between ESM2G and ESM2M is that ESM2G uses a spatially variable isopycnal tracer diffusion

126 coefficient of 50-900 $m^2 s^{-1}$ with the buoyancy frequency and isopycnal slope while
127 ESM2M uses a constant one of 600 $m^2 s^{-1}$. This coefficient determines the lateral stirring
128 by mesoscale eddies of all prognostic tracers in the model, including nutrients, oxygen,
129 phytoplankton, temperature and salinity. In the absence of feedbacks on circulation, we
130 would expect higher isopycnal tracer diffusion coefficients to prevent nutrients from
131 accumulating in stagnant low-latitude oxygen minimum zones, reducing the productivity
132 of the low latitudes and raising productivity in high latitudes. Mesoscale eddies also
133 produce advective fluxes. Following Gent and McWilliams (1990), these fluxes are
134 represented as flattening isopycnal surfaces, using a spatially variable thickness diffusion
135 coefficient that depends on the local thermal wind shear (Gnanadesikan et al., 2006).
136 ESM2G has a slightly larger range for this coefficient ($10 m^2 s^{-1}$-900 $m^2 s^{-1}$) than ESM2M
137 (100-800$m^2 s^{-1}$). In general, higher thickness diffusion would be expect to reduce mixed
138 layer depths, particularly in high latitudes (Gnanadesikan et al., 2007).
139 The models handle mixed layers differently. ESM2M uses the KPP mixed layer
140 scheme of Large et al. (1994). However, the effective mixed layer depth in this scheme is
141 the thickness of the topmost box, which is of order 10m. By contrast, ESM2G uses the
142 four-layer, total kinetic energy budget, bulk scheme described in Hallberg (2003) in
143 which the top two variable-density layers are completely mixed with respect to tracer but
144 not with respect to velocity and two transition layers govern exchange with the isopycnal
145 interior. ESM2G thus allows for a continuously varying mixed layer depth which can
146 take any value greater than 2m and should thus be superior to ESM2M in treating such
147 shallow mixed layers. However, insofar as processes such as breaking waves are not
148 included the result may be to make ESM2G too sensitive to addition of buoyancy under

calm winds. Additionally, the use of variable-depth mixed layers does introduce some complications. When the mixed layer shallows as a result of surface buoyancy addition, the water detrained from the mixed layer may not be at a density that corresponds to that of one of the interior layers. To avoid dividing the detrained water between two interior density layers (essentially "unmixing" the detrained fluid), the model instead adds the detrained water to a variable-density interior transition layer, which detrains slowly into a second variable-density transition layer which in turn detrains into a constant-density interior layer when it matches the density of this layer. This scheme allows for much smoother interaction between the surface layers and the interior, so that water detrained from a rapidly lightening surface layer will eventually be distributed over the entire range of densities found at the surface. However, it lacks resolution of the sub-mixed layer euphotic zone under conditions of weakly-stratified interior layers- the primary shortcoming of isopycnal models.

Dunne et al. (2012) examine the physical differences between ESM2M and ESM2G. We briefly summarize their results here. They find that the differences in patterns of radiative biases (shortwave albedo at top of atmosphere, downward shortwave radiation at surface, surface albedo) are very similar between the two models. Biases in sea surface temperature and salinity are also similar, though ESM2G tends to have somewhat larger RMS biases than ESM2M. In the ocean interior, however, the models differ considerably. ESM2M tends to drift warm, producing a thermocline that is excessively deep. ESM2G, by contrast, tends to drift slightly cold in the deep ocean and to produce a thermocline that is somewhat too thin. Overturning circulations within the two models are broadly similar in magnitude. The annual-mean maximum Atlantic

overturning in density space at 26N in ESM2G is 20.5 Sv+/-1.5Sv while in ESM2M it is 21.1 Sv +/-1.5Sv. Both models compare relatively well with the latest observational estimates from RAPID that give a maximum overturning at 26.5ºN equal to 18.7 +/- 4.8 Sv (Rayner et al., 2011). A somewhat more powerful way of assessing the overall ventilation of the Atlantic is the ideal age, a tracer that is set to zero at the surface and ages at a rate of 1 yr/yr below the surface (Thiele and Sarmiento, 1990). Ideal age measures the average time required to reach an interior box from the surface and accounts for diffusive pathways and advective pathways associated with the overturning. ESM2G produces a relatively old mass of intermediate waters within the Atlantic, with peak ages reaching 800 years in the Southern Hemisphere, overlying a relatively well-ventilated deep ocean in which ages range from 100-500 years. ESM2M produces a more-ventilated intermediate water, with ages of around 600 years, but has much shallower ventilation in the North Atlantic, so that the deep waters there are significantly older, ranging from 300-500 years. In both models a significant fraction of the Northern overturning is fed from the Southern Ocean, but the northern and southern cells are deeper in ESM2G than in ESM2M, with the northern cell realistically penetrating all the way to the bottom in the North Atlantic in ESM2G.

b.) Biogeochemical model

The ocean biogeochemical model used in both ESMs is the Tracers of Ocean Phytoplankton with Allometric Zooplankton (TOPAZ) model version 2. A prototype is described in Dunne et al. (2010). This model resolves three types of phytoplankton: small,

large and diazotrophs. Additionally, diatoms are diagnosed as a fraction of large phytoplankton. Phytoplankton growth is a function of limitation from multiple locations and light. Ammonia limitation is the simplest of these, and is handled using a simple Michaelis-Menten formulation, so that when it is the limiting nutrient the growth rate μ

$$(1)\ \mu \propto \frac{NH_4}{K_{NH4} + NH_4}$$

As described in more detail in Dunne et al. (2010), nitrogen limitation is a combination of the simple ammonia limitation above and nitrate limitation (which is suppressed by high levels of ammonia), while phosphorus and iron limitation are handled by considering the cellular quotas of these nutrients.

Small phytoplankton tolerate lower levels of iron, phosphate, ammonia/nitrate, and the rate of grazing on them (G) goes as their concentration

$$(2)\ G = \lambda_o e^{kT} (S / P_*)$$

where λ_0 is a grazing rate at 0C, k parameterizes a temperature-dependent increase in this grazing rate, T is the temperature in C, S is concentration of small phytoplankton and P_* is a scale factor. As a result, the steady-state concentration of these plankton (found by setting the growth rate in (1) equal to the grazing rate in (2) increases linearly for very low concentrations of limiting nutrients. However as nutrients become abundant, a similar absolute variation in concentration results in little change in growth and thus in biomass.

Large phytoplankton, such as diatoms and green algae, require higher ambient levels of phosphorus, nitrogen and iron than the small plankton (with half saturation constants three times larger), but are grazed according to a grazing law

(3) $G = \lambda_o e^{kT} (L / P_*)^{1/3}$

where L is the concentration of large phytoplankton and the other terms are as in (1). Thus at steady-state and very low nutrient concentrations, doubling the concentration of limiting nutrients will double the concentration of small plankton and increase the productivity by a factor of 4, but increase the concentration of large plankton by a factor of 8 and the grazing rate by a factor of 16. The great advantage of this allometric (size-dependent) grazing law is that it requires the estimation of relatively few parameters, which can be fit from available data (Dunne et al., 2005). The fraction of the large production associated with diatoms is determined simply as the Michaelis-Menten silicate limitation term with a half saturation coefficient of 1 μmol kg^{-1}. In the North Atlantic, diatoms and non-diatoms have similar temporal behavior in our model, with diatoms dominating the large plankton biomass, although this is not the case in other basins. We will therefore focus on the diatom biomass in this work. The final class represents diazotrophs which require phosphate and iron but can fix nitrogen, have low growth rates, and are grazed similarly to large phytoplankton. Diazotrophs play an important role in the nitrogen cycle, but account for a small fraction of the total primary production. We will not consider their impacts in the remainder of this paper.

As described in Dunne et al. (2012), the models are initialized from observed temperatures, salinities and nutrients and run with 1860 radiative conditions for over 1000 years. At the end of this spin-up period drifts in both models are relatively small. The 1860 Control integrations with fixed atmospheric greenhouse gasses and aerosols start at this point at the end of the spin-up period. Our analysis is based on the first 500 years of the 1860 Control runs.

The differences in physical forcing do result in some key differences in nutrient fields. As illustrated in Fig. 1, ESM2G shows a more realistic range in surface nitrate than ESM2M for the North Atlantic. In the data, the region where nitrate levels remain above the model's half-saturation constant for nitrogen uptake by diatoms (6 μM) year-round shrinks to a small region southeast of Greenland by August. ESM2G also shows nitrogen drawdown over this broad region, but the area where nutrients are retained is shifted to the Northeast corner of the main basin. By contrast, ESM2M retains high nitrogen over a much larger region (Fig.1e,f) so that a much smaller fraction of the subpolar Atlantic is nutrient limited at the end of the summer. One reason for this difference appears to be light limitation, the depth-averaged light in the shallower mixed layer is 20-30 W/m^2 higher in ESM2G than in ESM2M throughout the spring months in the northwest Atlantic.

3. Atlantic temperature variability in the two models

We begin by examining a 500-year time series of the AMO index in ESM2M and ESM2G (Fig. 2a). Both models show significant variability at multidecadal time scales, though the amplitude of the variability is significantly larger in ESM2G (standard deviation of 0.15°C) than ESM2M (standard deviation of 0.075°C). ESM2G also shows much more skewed variability toward intense cold periods. The long cold period towards the end of the time series ends in the middle of the 6^{th} century and does not represent a long-term trend. However, it is noteworthy that the coldest periods in ESM2G correspond to a Northwest Atlantic in which sea ice stretches south to the latitude of northern Nova

Scotia and east to the longitude of Greenland, an extent much larger than has been recorded during the historical record. This may represent a failure of the historical record to capture the true variability. During the first two centuries of the run, the range of wintertime sea ice cover in ESM2G actually compares well with observational records (Hill and Jones, 1990). Alternatively, the larger range in ESM2G may be the result of the more dynamic mixed layer in this code being overly sensitive to buoyancy addition.

Regressing the AMO index onto the decadally smoothed SST (Fig.2b,c) shows that the most intense temperature signals in both models are concentrated in the Northwest Atlantic and in the Greenland Sea, with a change of 1°C over the entire basin corresponding to changes in excess of 4°C over large swathes of these regions. Both models also show similar patterns of changes south of 45°N, with a cold anomaly off of North America and two tongues of warm anomalies emanating into the subtropical gyres. Local differences between these patterns likely arise from different representation of the path of the North Atlantic Current. In both models a 1°C change in basin-mean temperature corresponds to a significantly smaller warming at low latitudes. The concentration of the highest regressions in the Northwest Atlantic is common to many climate models (Ting et al., 2011). It should be noted that as one progresses to longer and longer temporal averages (corresponding to periods more characteristic of the data than of most climate models) the warming signal becomes more uniform over the basin. Observational estimates of AMO variability reported in Ting et al. (2011) show a pattern that is consistent with such longer temporal averages, though it is unclear how much of this is due to undersampling of the convective regions in the northwest Atlantic. By contrast, Stein (2007) finds a much larger signal in the northwest Atlantic, both using in-

situ temperatures at Greenland and the NOAA extended SST reconstruction. Regressing the AMO index vs. SSS (Fig 2d,e) shows that in addition to the signal in temperature, there is also a strong signal in salinity in the subpolar gyre, with warmer temperatures corresponding to higher salinities. As with temperature, this signal is concentrated in the Labrador Sea, but also propagates out into the main Atlantic basin.

Regression coefficients for salinity are about half those for temperature, so that a 0.5°C change in AMO index results in a peak change in annual mean SST of about 2.5°C and ~1 PSU. At the low temperatures found in the subpolar Atlantic, this implies that a higher AMO index is associated with denser surface waters in the Northwest Atlantic. One would thus expect that a high AMO index would be associated with deeper mixing. Fig. 3 shows the correlation between AMO index and the decadally smoothed log of the mixed layer depth during March (Fig. 3a and c) and August (Fig. 3 b and d) for the two models. In both models, a warmer Atlantic is correlated with deeper wintertime mixed layers throughout the Northwest Atlantic, but with a notably different pattern during the summer months. The spatial extent of enhanced wintertime mixing is much greater in ESM2G than in ESM2M.

The relationship between the AMO index and salinity in Fig.2 and mixed layer depth in Fig. 3 suggests a possible connection with the thermohaline circulation. While such a connection does exist in both ESM2M and ESM2G it is expressed quite differently in the two models. As shown in Fig. 4a the relationship between the standardized AMO index (anomaly divided by the standard deviation) and standardized overturning anomalies is quite good in ESM2G. Overturning anomalies computed in density space at 26ºN and 45ºN show an obvious relationship with the AMO index, and a lag correlation

(solid lines, Fig. 4c) shows the overturning at 45ºN leading the AMO by about 4 years and the overturning at 26ºN leading by about 2 years. Peak correlations are very high, exceeding 0.9 for the overturning at 45ºN. The phase relationship is consistent with an increasing in the overturning driving warming of the Atlantic. By contrast, the relationship between AMO index and overturning in ESM2M is much weaker with correlations peaking only at a level of 0.5 or so. It is notable that the overturning in ESM2M does exhibit a similar phase relationship to the AMO index as in ESM2G.

The differences between the models can also be seen in the spectra of the standardized AMO index and overturning anomalies (Fig. 4d). Not surprisingly given the high correlation between the overturning and AMO index, ESM2G shows consistent spectra between the three time series, with a broad peak at periods between 20-90 years. ESM2M shows rather different spectra for the AMO index (which has a peak at lower frequencies) and the overturning (with a relatively strong peak at around 20-30 years period).

While a complete analysis of the feedbacks responsible for the difference in overturning behavior in the two models is beyond the scope of this paper, we can make some preliminary statements about mechanisms that may contribute to the differences. If one thinks of the overturning as a pressure-driven oceanic circulation, the key question that arises is why the driving pressure gradients vary. The fact that the overturning is associated with saltier, warmer waters in high latitudes suggests that one focus should be explaining changes in the salinity on decadal time scales. Examining the correlations between decadally smoothed overturning and net water flux in the two models (colors in Fig. 5a,c), we see that higher overturning is correlated with excess evaporation over the

center of the subpolar gyre and excess precipitation/ice melt/runoff along the edge of Greenland and the Labrador sea in both models. The correlations are much higher in ESM2G than in ESM2M. In both models, hydrological feedbacks would seem to enhance surface salinity anomalies in the convective regions. In ESM2G a 1Sv change in overturning is associated with a 70 mm/yr decline in net water flux over region 50W-40W and 45-55N with a correlation coefficient of -0.57. Such a change represents a substantial fraction of the 511 mm/yr of net water added to the ocean annually in this region. Over the course of a decade, an anomalous flux of this size would change the salinity of the top 100m of the ocean by 0.25 PSU. In ESM2M the same region has a correlation coefficient of -0.21, and a 1 Sv change in overturning is associated with a much smaller -16 mm/yr change in water flux.

Annual mean wind stresses in both models show high overturning to be connected with more flow out of the Arctic, but in ESM2G this flow is connected with a more intense anticyclonic flow off Greenland (consistent with a westward movement of the Icelandic low), whereas in ESM2M the connection extends out towards Europe. This means that in ESM2G, a high overturning is associated with much stronger Ekman upwelling of salty warm deep water in the Northwest Atlantic than in ESM2M, potentially adding a second mechanism for reinforcing surface salinity anomalies.

If we ask how such salinity anomalies would get established in the first place, we get a slightly different picture. Correlating annual mean water and momentum fluxes with changes in the overturning (Fig. 5b,d) we see that the correlation between the net water flux and the overturning trend (in Sv/yr) is much smaller than it is for the overturning. Moreover it is also of the wrong sign over much of the Northwest Atlantic, with

355 increasing overturning associated with more water entering the ocean (a similar picture
356 emerges in ESM2G if one simply uses the salinity from 50-40°W and 45-55°N).
357 Increasing overturning in both models is associated with a cyclonic atmosphere
358 circulation south of Iceland. This is broadly consistent with recently published work by
359 Hakkinen et al. (2011) who relate the AMO index to changes in the 2nd PC of SLP, which
360 has a similar center of action to what we see in both ESM2M and ESM2G. Comparison
361 of their figures 1B and 2B show that when the detrended AMO index is increasing (1920,
362 1990s) there is a positive wind stress curl anomaly over this region, whereas the decrease
363 in the same index in the late 1950s and 1960s is associated with lower wind stress curl. In
364 ESM2G the anomalous cyclonic circulation is stronger and extends further to the south
365 than in ESM2M. Insofar as decadal salinity anomalies are important drivers of
366 overturning variability, the suggestion from Fig. 5 is that the two models differ in
367 relatively subtle ways in how such salinity anomalies are generated by winds over the
368 North Atlantic and how effective atmospheric feedbacks are at maintaining them.
369

370 **4. Relationship between AMO index and biological variability**
371

372 Using output from GFDL's prototype ESM2.1, Gnanadesikan et al., (2011)
373 showed that the variability in the biomass of large phytoplankton was much more
374 extreme than total phytoplankton biomass, both in the annual mean and by seasons. The
375 reason for this is clear from equation (2)- in order for grazing to match similar relative
376 changes in phytoplankton growth rate, much larger changes are required for large
377 phytoplankton than for small phytoplankton. Figure 6a shows the coefficient of

variability for decadal variation in diatom biomass in ESM2G (colors) and ESM2M (contours) respectively. A striking result is how little variability there is in annual-mean biomass (Fig. 6a) over the majority of the subpolar North Atlantic, with coefficients of variation in both models less than 0.1. The exception in ESM2G is in the northwest Labrador Sea and off of Norway. This lack of interannual variation is also consistent with recent work by Henson et al. (2009) examining the interannual variability in satellite-estimated primary productivity.

However, when we examine the coefficient of variation of decadally smoothed biomass in each month much larger variations are seen. Fig. 6b-d shows the coefficient of variation for diatom biomass decadally smoothed over April, July and October respectively. Large coefficients of variation are seen throughout the basin in April in both models, with the highest values in the Labrador and Norwegian Seas. In July and September ESM2M shows higher variability at low latitudes. By contrast ESM2G shows most variability at high latitudes with values greater than 0.4 seen in the Labrador Sea, off Norway and at the edge of Bay of Biscay shelf.

We can examine which of these regions shows the best correlation with the meridional overturning circulation by performing a composite analysis in which we examine the differences between those times when the overturning circulation or AMO index is more than one standard deviation above its mean and those times when the corresponding index is more than one standard deviation below its mean (note that because of the lag between the overturning and AMO index, these composites will correspond to slightly different years). Composites for ESM2G are shown in Figure 7 with colors showing the log of the ratio of large diatom biomass between high and low

overturning periods and contours showing the difference in nitrate concentration from April to October. A clear pattern emerges during the summer months whereby nitrate concentrations are higher in the Labrador Sea and lower in the eastern Atlantic, and diatom biomass ratios follow this general pattern. The pattern of nitrate change mimics the pattern of mixed layer depth changes in Fig.3 throughout subpolar latitudes. Note that the variability off of Norway is relatively uncorrelated with the overturning. Analysis of what drives this variability shows it to be related to the summertime depth of the transition layer. Essentially, times with low biomass correspond to times with shallow mixed layers, but very deep transition layers, so that each day's production is rapidly mixed below the euphotic zone. Given the likelihood that the signal off Norway in ESM2G is a numerical artifact of the lack of resolution below the mixed layer, we will not discuss it further in this paper.

The analogous picture for ESM2M (Figure 8) shows similar patterns of nutrient variability (higher nutrients in the Northwest Atlantic, lower in the Northeast under warm conditions), but the amplitude of variability is far smaller (1-2 μM rather than more than 6 μM). ESM2M exhibits much less variability in diatom biomass. Larger variability in diatom biomass in ESM2M relative to ESM2G is seen in April in the Greenland Sea, near a region which also sees higher variability in temperature and mixed layer depth.

The heterogeneity in diatom biomass variability seen across the basin and between the different models demonstrates that a simplistic view of how biomass and temperature are linked is unlikely to work. In the three subsections that follow we discuss three different regions where significant interdecadal variability in biomass is linked to

423 the basin-mean SST. We break these regions down by the ways in which diatom biomass
424 is limited. Because ESM2M shows so little variability we focus on ESM2G.
425
426 b.) Nutrient-limited, convectively supplied (Labrador Sea, ESM2G)
427
428 We begin by looking at an area to the west of Greenland, stretching across
429 longitudes 60ºW-50ºW and latitudes 60-64ºN shown by the red box in Figure 7b. As
430 shown in Fig 7, in ESM2G the diatom biomass is much higher in this region from April
431 through August during warm periods than during cold periods, and nutrients are higher as
432 well. A composite of the annual cycle of diatom biomass in this region during warm and
433 cold periods (Fig. 9a) shows that the biomass peaks later and persists longer under warm
434 periods (solid green lines) than under cold periods (solid blue lines). The relationship is
435 similar when the overturning in density space at 45ºN is used to segregate different
436 periods (dashed lines). We can isolate the relevant mechanism driving these differences
437 by looking at the ratio of various fields under the different regimes. As seen in Fig. 9b,
438 the high AMO/overturning regime off of Greenland is associated with lower diatom
439 biomass/light and higher mixed layer depth and nutrients during the winter months.
440 During the spring, light and mixed layer depths are essentially the same, but high
441 nutrients persist through the summer and result in higher levels of diatom biomass
442 throughout the summer months.
443 The relationships suggested by the composite analysis can also be seen through
444 looking at scatterplots between summertime diatom biomass and other fields over time
445 (Fig. 10). Figure 10a shows the relationship between diatom biomass in June averaged

over the West Greenland area and mean mixed layer depth in the previous March, when mixed layers in this region are at their deepest. The correlation between the two is 0.76 without decadal smoothing and 0.89 with it. Note that the diatom biomass during June ranges over a factor of 5. By contrast, the correlation between June mixed layer depth and diatom biomass is much weaker (0.13 without decadal smoothing and only 0.43 with it). There is clearly a strong relationship between June biomass and June nitrate (red points, Fig. 10b) with a correlation coefficient of 0.97. Given that the nitrate concentrations are varying across the range where limitation is expected to occur, this correlation is unsurprising. The approximately 5 μM range in June nitrate is mirrored by a similar range in concentrations during March (black points, Fig. 10b) with a correlation between June nitrate concentration and March nitrate concentration of 0.88.

Plotting the diatom biomass vs. the standardized overturning anomaly and standardized AMO index (Fig 10c), we see a tighter relationship between the overturning and the diatom biomass (with a lag-0 correlation of 0.82) than with the AMO index (0.71). In fact the diatom biomass leads the AMO index, by about 4 years (with a maximum correlation of 0.83), similar to the overturning. The lagged correlation analysis thus suggests that the relationship between diatom biomass and temperature in this region is actually secondary to the relationship with convection and overturning.

Finally, looking at the surface salinity (black points, Fig. 9d) and 200m salinity (red points Fig. 9d), we see that the variability in biomass is clearly related to salinity stratification. Time periods with high biomass are marked with high wintertime surface salinities, matching those at 200m, which vary relatively little. We note that the range in surface salinities of ~1.0 PSU (with most of the points lying between 33.6 and 34.4) is

actually quite consistent with the shorter time series reported in Belkin et al. (1998) in the West Greenland Current. High salinity in the Labrador Sea reduces stratification, allowing deeper convection, which brings up warm water and nutrients. In ESM2G, this results in alleviation of nutrient limitation during the summer months and allows for much higher biomass. In ESM2M, by contrast, nutrients stay high during the summer months and any variability in diatom biomass is driven by changes in mixed layer depth which have a much weaker relationship with average Atlantic temperatures (Fig. 3).

c.) Ice edge regime (60°W-55°W, 52°N-56°N)

Higher overturning is associated with more import of warm water into high latitudes. This can result in an earlier melt-back of sea ice during the spring, relieving light limitation on the mixed layer and producing an earlier spring bloom. This effect shows up particularly strongly off the northern coast of Labrador in ESM2G shown by the red box in Fig. 7a. As shown in Figure 9c, in this region high AMO index/overturning is associated with higher biomass and an earlier spring bloom. Plotting April diatom biomass vs. nitrate (Fig. 11a) shows some relationship (correlation coefficient of 0.53), but the range in biomass is far larger in a relative sense than the range in nutrients, which are at levels at which nitrate is only mildly limiting. By contrast, the relationship between biomass and light is much tighter (Fig 11b), with the sevenfold range in biomass corresponding to a comparable range in light and a correlation coefficient of 0.94. The variation in light levels can largely be explained by variations in ice extent (Fig. 11c), which are anticorrelated with April diatom biomass (-0.94).

Comparing the AMO index (solid) and overturning (dashed) curves in Figure 9d, one notices a more extreme response in the former. In contrast to the previous region considered, the correlation between spring biomass off the Labrador coast is better correlated with the AMO index (0.82) than with the overturning at 45°N (0.64). When the overturning leads the spring diatom biomass by 4-6 years the correlation rises to around 0.80. The scenario suggested by these analyses is one where an increase in overturning leads to a warming of the Northwest Atlantic, melting back sea ice during the spring and leading to an earlier spring bloom. Conversely, a decrease in overturning leads to less heat being brought to the surface in the winter, more sea ice cover and light limitation during the spring and a later spring bloom.

d.) Nutrient-limited advective supply

Biscay Plain (12°W-10°W,44°N-52°N)

A final region which shows a strong relationship with the overturning is Northeast Atlantic off the continental shelves of France and Ireland shown by the red box in Fig. 7c. While we chose this region because it shows strong variability in the fall bloom, observations also show strong blooms along the shelf edge (Garcia-Soto and Pingree, 2009). In this region, warm/high overturning conditions are found to give lower diatom biomass (Figure 9e,f) and surface nitrate (Figure 9f). Light and mixed layer depths appear to have a relatively minor impact on the growth rates. The diatom biomass varies much more when overturning is used to make the composites than when the AMO index is used. This suggests that, as is the case for the West Greenland coast, it is the variability

515 in the overturning that drives the diatom variability, rather than the (lagged) variation in
516 temperatures.

517 The driving mechanism for the variability in the Northeast Atlantic in ESM2G is
518 the persistence of higher levels of nitrate into the summer and autumn months.
519 Examination of the nutrient fields shows that this is associated with eastward shifts of
520 the edge of the high-nutrient subpolar gyre. As shown in Fig. 12, high biomass in this
521 region is correlated with a plume of high surface nitrate along the gyre edge (Fig. 12a).
522 These correlations hug the edge of a high nutrient plume (Fig. 12b) down to several
523 hundred meters and are also seen in temperature (Fig. 12c) and density (Fig. 12d). The
524 picture that emerges is one of variations in the central track of high nutrient mode waters
525 in the Northeast Atlantic. As this track broadens and shifts to the east higher nutrients are
526 available to diatoms in surface waters, allowing them to persist through the summer
527 months.

528

529 **5. Conclusions**

530

531 We show that Earth System Models are capable of simulating relationships
532 between phytoplankton biomass in various parts of the North Atlantic mean temperature
533 of the Atlantic as described by the AMO index. Such relationships however, are likely to
534 be spatially heterogeneous because of the competing impacts of light and nutrient
535 limitation and are not robust across models. A higher AMO index in both models is
536 associated with a stronger overturning, which results in more convection and nutrient
537 supply during winter months. In the ESM2G model, this increased nutrient supply results

in significantly higher diatom biomass throughout the year. Such a relationship between higher salinities, temperatures and biomass is particularly interesting given that there is evidence for significant variability of cod populations in this region. Work on Pacific cod (Laurel et al., 2008, 2011) shows that while higher temperatures in the absence of food would be expected to reduce larval survival, higher temperatures in the presence of food produce much larger larval cod at two months past fertilization.

ESM2M, by contrast, does not show strong variability in biomass despite variability in nutrients that has the similar absolute value. This is because nutrients are unrealistically high in this region throughout the year, as mixed layer light is systematically lower in the level-coordinate model, and so the nutrient variability does not drive significant variability in biomass. Variability in subpolar diatom biomass in ESM2M is in general smaller than in ESM2G and is more tightly related to mixed layer depth, which in turn is more weakly related to basin-mean SST.

It is unclear which of the two models is "most realistic". On the one hand, the shallower mixed layers in ESM2G do allow for a more realistic nutrient simulation than in ESM2M.On the other hand, it is possible that these mixed layers are too sensitive to freshening, and that the shallower mixed layers in ESM2G yield better nutrients because they compensate for biases in the biogeochemical model. For example, given a different representation of photoadaptation or of light absorption, it is possible that the mean nutrient simulation in ESM2M could be made to look more like ESM2G. Better proxy constraints on sea ice cover over the entire Holocene (e.g. Solignac et al., 2004), particularly in regions which today are ice-free, would help to constrain this uncertainty. At least one coastal record (Levac, 2001) does suggest the existence of significant

intervals during the Holocene where wintertime sea ice extended much further south along the North American coast than it does today, and that such periods were associated with fresh anomalies.

In regions such as this, where variability is linked to the overturning rather than to the mean North Atlantic SST, interannual variability may not be a good indicator of the response under global warming. Off West Greenland, warm periods are associated with saltier surface water, deeper convection and more overturning, whereas global warming is expected to warm the Atlantic as a whole, but to decrease overturning and convection. Such differences highlight the importance of linking biological variability to physical mechanisms rather than merely to statistical modes of SST variability.

Both models do show variability in ice-edge regions associated with the AMO index during the spring bloom. These regions do not necessarily vary in the same way as adjoining regions, as illustrated by the Labrador Sea in ESM2G, where the ice edge experiences an earlier bloom but the open-ocean convective region experiences a later spring bloom. We note that these regions may respond to global warming as they do to an increase in the AMO index, and may also represent regions where there is some predictability, insofar as the AMO index lags the overturning circulation at 45°N.

The spatial heterogeneity of the biogeochemical response of the Atlantic to changes in overturning (particularly in ESM2G) may help explain why fisheries in different parts of the Atlantic show different responses to decadal-scale variability. An additional complication is that the response of organisms at higher trophic levels to such changes in overturning will depend strongly on details of their life history. In particular, organisms whose spawning is tied to particular times of year may be especially

584 susceptible to shifts in the timing of spring or fall blooms. Such details need to be
585 considered by climate scientists in particular when linking variability in their models to
586 observed changes in fisheries.

587 **Acknowledgements:** We thank Ron Stouffer, Marie-Aude Pradal and Bob Hallberg for
588 useful comments on an earlier version of this manuscript. AG received support for this
589 work under DOE Grant DE-SC0007066.

590

591 **References**

592 Belkin, I.S., Levitus, S., Antonov, J., Malmberg,S.-A., 1998. "Great salinity anomalies"
593 in the North Atlantic, Progress in Oceanography, 41, 1-68.

594 Collie, J.S., Wood, A.D., H.P Jeffries, H.P., 2008. Long-term shifts in the species
595 composition of a coastal fish community, Can. J. Fisheries and Aquatic Sci., 65,1352-
596 1365, 2008.

597 Delworth, T.L., Mann, M.E., 2000. Observed and simulated multidecadal variability in
598 the Northern Hemisphere, Climate Dynamics, 16, 661-676, 2000.

599 Delworth, T.L., Broccoli, A.J., Rosati, A., Stouffer, R.J., Balaji, V., Beesley, J.A., Cooke,
600 W.F., Dixon, K.W., Dunne, J.P., Dunne, K.A., Durachta, J.W., Findell, K.L., Ginoux,
601 P., Gnanadesikan, A., Gordon, C.T., Griffies, S.M., Gudgel, R., Harrison, M.J., Held,
602 I.M., Hemler, R.S., Horowitz, L.W., Klein, S.A., Knutson, T.R., Kushner, P.J.,
603 Langenhorst, A.R., Lee, H.-C., Lin, S.-J., Lu, J., Malyshev, S.L., Milly, P.C.D.,
604 Ramaswamy, V., Russell, J., Schwartzkopf, M.D., Shevliakova, E., Sirutis, J.J..
605 Spelman, M.J., Stern, W.F., Winton, M., Wittenberg, A.T., Wyman, B., Zeng, F.,

606 Zhang, R., 2006. GFDL's CM2 global coupled climate models: Part 1- Formulation
607 and simulation characteristics, J. Climate, 19, 643-674.
608 Dulvy, N.K., Rogers, S.I., Jennings, S., Stelzenmuller, V., Dye, S.R., Skjoldal, H.R.,
609 2009. Climage change and deepening of the North Sea fish assemblage: a biotic
610 indicator of warming seas, J. Applied Ecology, 45, 1029-1039, doi: 10.1111/j.1365-
611 2664.2008.01488
612 Dunne, J.P.,Armstrong, R.A., Gnanadesikan, A., Sarmiento, J.L., 2005. Empirical and
613 mechanistic models of particle export, Global Biogeochem. Cycles. 19, GB4026,
614 doi:10.1029/2004GB002390.
615 Dunne, J.P., John, J.G., Adcroft, A.J., Griffies, S.M., Hallberg, R.W., Shevliakova, E.N.,
616 Stouffer, R.J., Cooke, W., Dunne, K.A., Harrison,M.J., Krasting, J.P., Levy,H.,
617 Malyshev, S.L., Milly, P.C.D., Phillips, P.J., Sentman, L.A., Samuels, B.L., Spelman,
618 M.J., Winton, M., Wittenberg, A.T., Zadeh, N., 2012. GFDL's ESM2 global
619 coupled climate-carbon Earth System Models Part I: Physical formulation and
620 baseline simulation characteristics, J. of Climate in press.
621 Enfield, D.B., Mestaz-Nunez, A.M., Trimble, P.J., 2001. The Atlantic Multidecadal
622 Oscillation and its relation to rainfall and river flows in the continental U.S., Geophys.
623 Res. Lett., 28, 2077-2080.
624 Ferrari, R., Griffies, S.M., Nurser, A..Vallis,G. 2010. A boundary-value problem for the
625 parameterized mesoscale eddy transport. Ocean Modelling, 32, 143–156.
626 Fox-Kemper, B., Danabasoglu,G., Ferrari, R., Griffies, S.M., Hallberg, R.W., Holland,M.,
627 Peacock, S., Samuels, B., 2011. Parameterization of mixed layer eddies. III: Global

implementation and impact on ocean climate simulations. Ocean Modelling, doi:10.1016/j.ocemod.2010.09.002.

Garcia, H.E., Locarnini, R.A., Boyer, T.P., Antonov, J.I., 2006. World Ocean Atlas 2005, Volume 4: Nutrients (phosphate, nitrate, silicate). S. Levitus, Ed. NOAA Atlas NESDIS 64, U.S. Government Printing Office, Washington, D.C., 396 pp.

Garcia-Soto, C., Pingree,R.D., 2009. Spring and summer blooms of phytoplankton (SeaWiFS/Modis) along a ferry line in the Bay of Biscay and western English Channel, Continental Shelf Res., 29,1111-1122.

Gnanadesikan, A., Dixon, K.W., Griffies, S.M., Balaji, V., Barreiro, M., Beesley, J.A., W.F. Cooke, W.F., Delworth, T.L., Gerdes, R., Harrison, M.J., Held., I.M., Hurlin, W.J., Lee, H.C., Liang, Z., Nong, G., Pacanowski, R.C., Rosati,A., Russell, J.L., , Samuels, B.L., Song, Q., Spelman, M.J., Stouffer, R.J., Sweeney, C., Vecchi, G., Winton, M., Wittenberg, A., Zeng, F., Zhang, R., Dunne, J.P., 2006. GFDL's CM2 global coupled climate models-Part 2: The baseline ocean simulation, J. Climate, 19, 675-697.

Gnanadesikan, A., Anderson,W.G., 2009. Ocean water clarity and the ocean general circulation in a coupled climate model, J. Phys. Oceanogr., 39, 314-332.

Gnanadesikan, A., Dunne, J.P., John,J., 2011. What ocean biogeochemical models can tell us about bottom-up control of ecosystem variability, ICES J. Mar. Sci, 68,1030-1044, doi:10.1093/icejms/fsr068.

Gnanadesikan, A., Griffies, S.M., Samuels, B.L., 2007. Effects in a climate model of slope tapering in neutral physics schemes, Ocean Modelling, doi:10.1016/ j.ocemod.2006.06.004, 16, 1-16.

651 Griffies, S. M., 2009. Elements of MOM4p1: GFDL Ocean Group Technical Report No.
652 6. NOAA/Geophysical Fluid Dynamics Laboratory, Princeton, USA, 444 pp.
653 Griffies, S.M., Gnanadesikan, A., Dixon, K.W., Dunne, J.P., Gerdes, R., Harrison, M.J.,
654 Rosati, A., Russell, J.L., Samuels, B.L., Spelman,M.J.., Winton,M., Zhang,R., 2005.
655 Formulation of an ocean model for global climate simulations, Ocean Science, 1, 45-
656 79.
657 Hakkinen, S., Rhines, P., Worthen, D.L., 2011. Atmospheric blocking and Atlantic
658 Multidecadal Ocean Variability, Science, 334,655-659.
659 Hallberg, R., 1995. Some aspects of the circulation in ocean basins with isopycnals
660 intersecting the sloping boundaries. Ph.D. thesis, University of Washington, 244 pp.
661 Hallberg, R., 2003. The suitability of large-scale ocean models for adapting
662 parameterizations of boundary mixing and a description of a refined bulk mixed layer
663 model. Near-Boundary Processes and Their Parameterization: Proc. ‘Aha Huliko‘a
664 Hawaiian Winter Workshop, Honolulu, HI, University of Hawaii at Manoa, 187–203.
665 Hallberg, R., Adcroft, A., 2009. Reconciling estimates of the free surface height in
666 Lagrangian vertical coordinate ocean models with mod-split time stepping. Ocean
667 Modelling, 29, 15-26.
668 Harrison, M.J., Hallberg,R.W., 2008. Pacific subtropical cell response to reduced
669 equatorial dissipation, J. Physical Oceanography, 38,1894-1912.
670 Henson, S.J., Dunne, J., Sarmiento, J.L, 2009. Decadal variability in North Atlantic
671 phytoplankton blooms, JGR Oceans, 114, C04013, doi: 10.1029/2008JC005139.
672 Hill, B.T., Jones, S.J., 1990. The Newfoundland Ice Extent and the Solar Cycle from
673 1860 to 1988, J. Geophys. Res., 95(C4),5385-5394.

674 Jensen, A.S., 1939. Concerning a change of climate during recent decades in the arctic
675 and subarctic regions from Greenland in the west to Eurasia in the east, and
676 contemporary biological and geophysical changes. Det Kgl. Danske Vid. Selskab
677 Biol. Meddr. XIV, 8. København.
678 Large,W. G., McWilliams, J.C., Doney, S.C., 1994. Oceanic vertical mixing: A review
679 and a model with a nonlocal boundary layer parameterization. Rev. Geophys., 32,
680 363–403.
681 Laurel, B.J., Hurst, T.P., Copeman, L.A., Davis, M.W., 2008. The role of temperature on
682 the growth and survival of early and late hatching Pacific cod larvae (Gadus
683 macrocephalus), J. Plankton Res., 30, 1051-1060.
684 Laurel, B.J., Hurst,T.P, Ciannelli, L., 2011. An experimental examination of temperature
685 interactions in the match–mismatch hypothesis for Pacific cod larvae, Can. J. Aquat.
686 Fish. Sci,. 68, 51-61.
687 Legg, S., Hallberg,R.W., Girton, J.B., 2006. Comparison of entrainment in overflows
688 simulated by z-coordinate, isopycnal and non-hydrostatic models. Ocean Modelling,
689 11(1-2), DOI:10.1016/j.ocemod.2004.11.006.
690 Levac, E. 2001., High-resolution Holocene paleolynogical record from the Scotia Shelf,
691 Marine Micropaleontology, 43, 179-197.
692 Nye, J.A., Link, J.S., Hare, J.A., Overholtz, W.J., 2009. Changing spatial distribution of
693 fish stocks in relation to climate and population size on the Northeast United States
694 continental shelf, Mar. Ecol. Progr. Ser. 393,111-129.
695 Rayner, D., Hirschi, J.J.M., Kanzow, T., Johns, W.E., Wright, P.G., Frajka-Williams, E,
696 Bryden, H.L., Meinen, C.S., Baringer, M.O.,Marotzke, J., Beal, L.M, S. A.

697 Cunningham, S.A., 2011. Monitoring the Atlantic Meridional Overturning
698 Circulation, Deep Sea Res., Part II, 58, 1744-1753.
699 Sarmiento, J.L., Slater, R.D., Dunne, J.P., Gnanadesikan, A., Hiscock, M.R., 2010.
700 Small-scale carbon mitigation by patch iron fertilization, *Biogeosciences*, 7, 3593-
701 3636.
702 Schlesinger, M.E., Ramankutty, N., 1994. An oscillation in the global climate system of
703 period 65-70 years, Nature, 367, 723-726.
704 Simmons, H. L., Jayne, S. R., St. Laurent, L.C., Weaver, A.J., 2004. Tidally driven
705 mixing in a numerical model of the ocean general circulation. Ocean Modelling, 6,
706 245–263.
707 Solignac, S., de Vernal,A., Hillaire-Marcel, C., 2004. Holocene sea surface conditions in
708 the North Atlantic- contrasted trends and conditions in the western and eastern sectors
709 (Labrador Sea vs. Iceland Basin), Quaternary Science Reviews, 23, 319-334.
710 Stein, M., 2007. Warming periods off Greenland during 1800-2005: Their potential
711 influence on the abundance of Cod (Gadus Morhua) and Haddock (Melanogrammus
712 aegelfinus) in Greenlandic waters, J. Northw. Atl. Fish. Sci., 39, 1-20.
713 Sundby, S., O. Nakken, O., 2008.Spatial shifts in spawning habits of Arcto-Norwegian
714 Cod related to multidecadal oscillations and climate change, ICES J. Mar. Sci., 65,
715 953-962.
716 Sutton, R.T., Hodson, D.L.R., 2005. Atlantic forcing of North American and European
717 summer climate, Science, 309, 115-118.

718 Ting, M., Kushnir,Y., R. Seager, R. ,Li, C., 2011. Robust features of Atlantic
719 multidecadal variability and its impacts, Geophys. Res. Lett., 38, L17705,
720 doi:10.1029/2011GL048712.
721 Thiele, G., J.L. Sarmiento, J.L., 1990. Tracer dating and ocean ventilation. Journal of
722 Geophysical Research 95, 9377-9371, doi: 10.1029/89JC01132.
723 Winton, M., R. W. Hallberg, and A.R.W., Gnanadesikan,A., 1998. Simulation of density-
724 driven frictional downslope flow in z-coordinate ocean models. Journal of Physical
725 Oceanography, *J. Phys. Oceanogr*. , 28(11), :2163-2174. 1998.
726 Zhang, R., Delworth, T.L.,2006 Impact of Atlantic multidecadal oscillations on
727 India/Sahel rainfall and Atlantic hurricanes, Geophys. Res. Lett., 33, L17712,
728 doi:10.1029/2006GL026267.
729

730 **Figure Captions**

731

732 **Figure 1:** Nitrate concentrations in mmol/m^3 in the North Atlantic. Observations are
733 from the World Ocean Atlas 2005 (Garcia et al., 2005). Models are results averaged over
734 years 1-500 of the 1860 Control Run. (A) Observations, March. (B) Observations, August.
735 (C) ESM2G, March. (D) ESM2G, August. (E) ESM2M March (F) ESM2M August. ‘

736

737 **Figure 2:** Atlantic temperature variability in ESM2M and ESM2G. (A) Unstandardized
738 AMO index (averaged SST between equator and 70°N in the Atlantic basin, decadally
739 smoothed). (B) Regression coefficient between the decadally smoothed local SST and the
740 AMO index (deg C/deg C) for ESM2G. A value of 2 means that the local SST change is
741 twice the AMO index. (C) Same as (B) for ESM2M. (D) Regression coefficient between
742 the decadally smoothed SSS and the AMO index (PSU/deg C) for ESM2G. A value of 2
743 means that a 1°C change in the AMO index would correspond to a 2PSU change in
744 surface salinity. (E) Same as (D) but for ESM2M.

745

746 **Figure 3:** Correlation between the AMO index and log of the mixed layer depth in ESM
747 control runs. (A) March, ESM2G. (B) August, ESM2G. (C) March ESM2M (D) August
748 ESM2M.

749

750 **Figure 4:** Relationship between the AMO index and density-space overturning in the two
751 ESMs. (A) and (B) show standardized anomalies of AMO index and overturning in
752 density space at 45 N and 26N for the first 600 years of the 1860 Control Run. (C)

753 Lagged correlations between AMO index and overturning with overturning lead in years.
754 (D) Spectra of overturning and AMO index. Solid lines in (C) and (D) are ESM2G,
755 dashed lines ESM2M.
756
757 **Figure 5:** Correlation between overturning streamfunction (left column) and its change
758 (right column) and precipitation minus evaporation (colors) and wind stress (vectors).
759 Top row shows results for ESM2G, bottom row for ESM2M.
760
761 **Figure 6:** Coefficient of variability (standard deviation/mean) of decadally smoothed
762 diatom biomass. Colors are for ESM2G, contours for ESM2M. (A) Decadally smoothed
763 diatom biomass. (B) Decadally smoothed April biomass. (C) Decadally smoothed July
764 biomass. (D) Decadally smoothed October biomass.
765
766 **Figure 7:** Composites of the difference in diatom biomass and surface nutrients between
767 high AMO index years and low AMO index years for the ESM2G model. Colors show
768 natural log of the ratio in diatom biomass, contours show the difference in dissolved
769 nitrate in mmol/m^3. Red boxes denote regions analyzed in the text. (a) April (b) June (c)
770 August (d) October.
771
772 **Figure 8:** Composites of the difference in diatom biomass and surface nutrients between
773 high AMO index years and low AMO index years for the ESM2M model. Colors show
774 natural log of the ratio in diatom biomass, contours show the difference in dissolved
775 nitrate in mmol/m^3. (a) April (b) June (c) August (d) October.

776

777 **Figure 9:** Composite seasonal cycle in three locations that show linkages between the
778 AMO index/overturning in density space and diatom biomass in ESM2G. Left column
779 shows diatom biomass under low AMO/overturning (blue lines) and high
780 AMO/overturning (green lines). Right column shows the ratio of various quantities
781 between high and low periods, solid lines when the AMO is used to discriminate, dashed
782 lines with the overturning at 45°N is used. Top row: West Greenland. Middle row:
783 Labrador Coast. Bottom Row: Bay of Biscay shelfbreak.

784

785 **Figure 10:** Scatterplot of decadally smoothed diatom biomass in June for West
786 Greenland in ESM2G. All plots show averages of 60°W-50°W and 60°N-64°N. (A)
787 March MLD, (B) March NO_3. (C) Standardized overturning anomaly at 45N (black) and
788 standardized AMO index (red). (D) Salinity at surface (black) and 200m (red).

789

790 **Figure 11:** Relationships between decadally smoothed biomass during the month of
791 April for the coast of Labrador (60-55°W, 52-56°N) in ESM2G. (A) April surface nitrate.
792 (B) April irradiance. (C) April sea ice extent. (D) Decadally smoothed overturning in
793 density space at 45°N and AMO index.

794

795 **Figure 12:** Relationships between decadally smoothed June diatom biomass above the
796 eastern Biscay plain (12°W-10°W, 44-52°N) and various hydrographic fields. (A)
797 Correlation with decadally smoothed nitrate at surface. (B) Colors: correlation with
798 decadally smoothed annual mean nitrate averaged from 44-52°N. Contours, mean nitrate

799 44-52°N. (C) Colors: correlation with decadally smoothed temperature averaged from
800 44-52°N. Contours, mean temperature 44-52°N. (D) Colors: correlation with decadally
801 smoothed potential density averaged from 44-52°N. Contours, mean potential density
802 averaged from 44-52°N.

Figure(s)

Click here to download Figure(s): comp_nuts.pdf

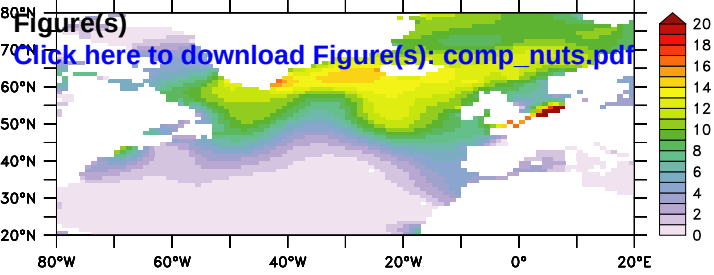

(A) Observed Nitrate, March

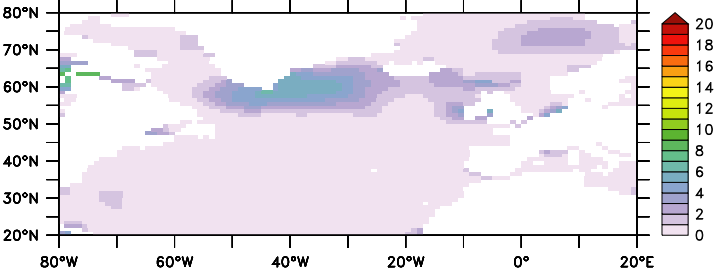

(B) Observed Nitrate, August

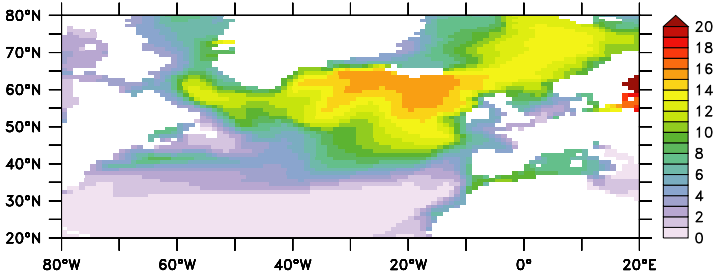

(C) ESM2G Nitrate, March

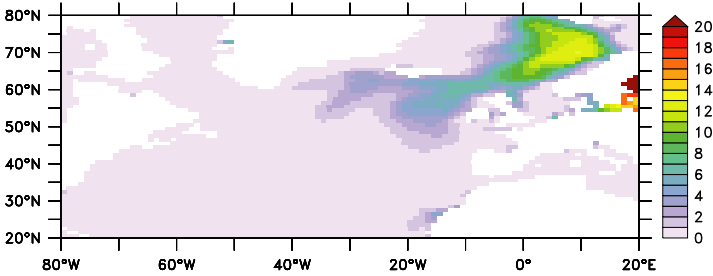

(D) ESM2G Nitrate, August

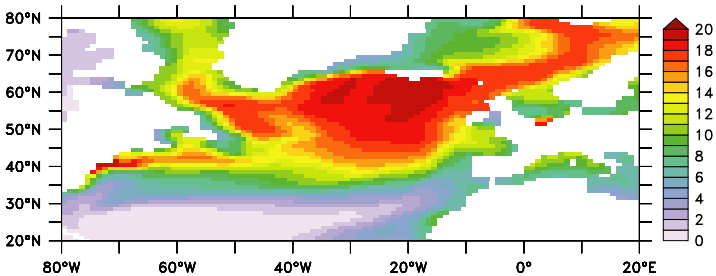

(E) ESM2M Nitrate, March

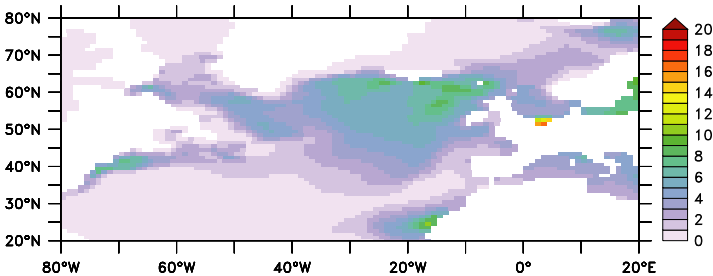

(F) ESM2M Nitrate, August

Figure(s)

Click here to download Figure(s): amo_sst_sss_corrs.pdf

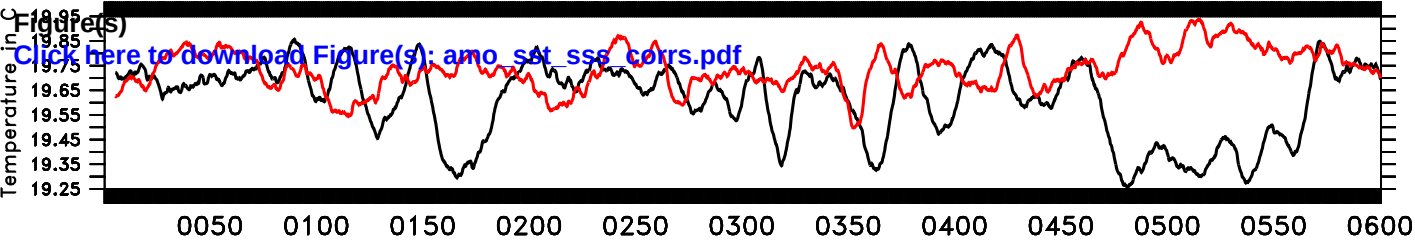

(A) Unstandardized AMO Index (ESM2G,ESM2M)

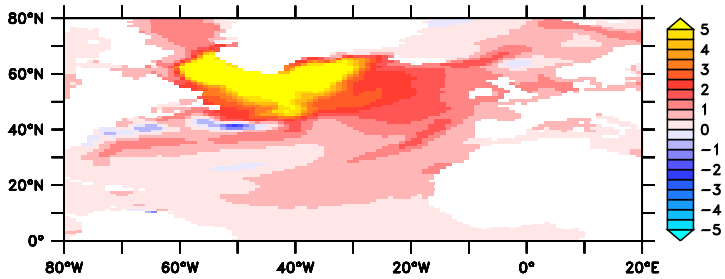

(B) AMOI–SST Regression: ESM2G

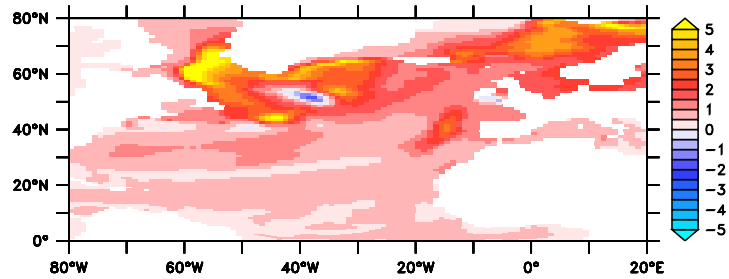

(C) AMOI–SST Regression: ESM2M

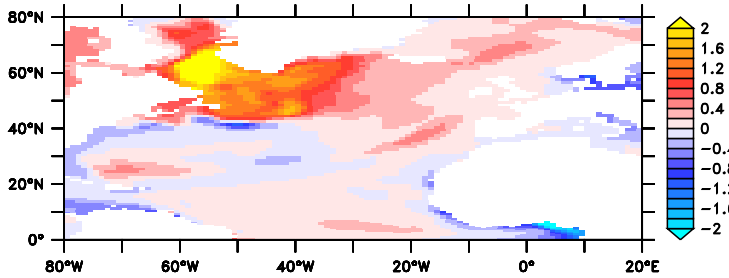

(D) AMOI–SSS Regression: ESM2G

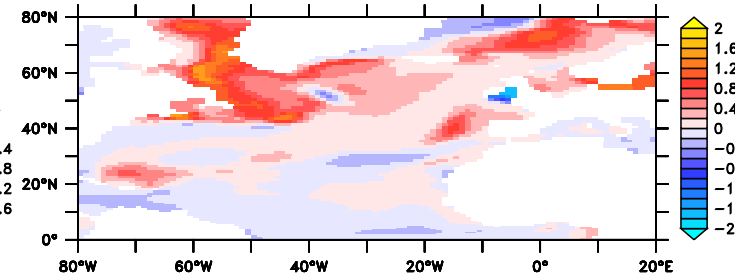

(E) AMOI–SSS Regression: ESM2M

Figure(s)

Click here to download Figure(s): amo_h_ML.pdf

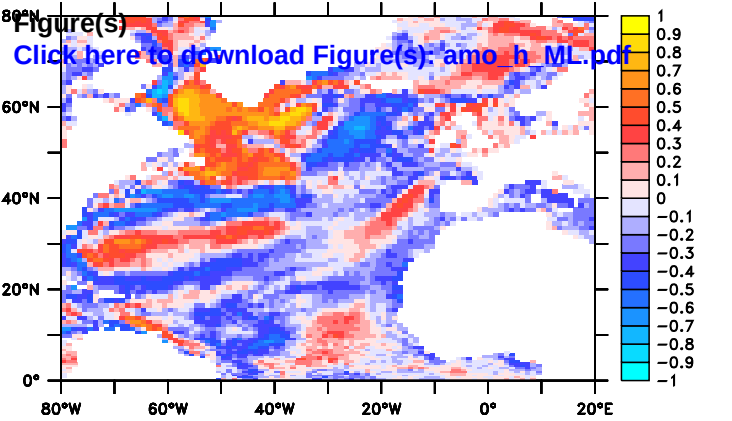

(A) $\log(H_{ML})$–AMOI Corr.: ESM2G, Mar

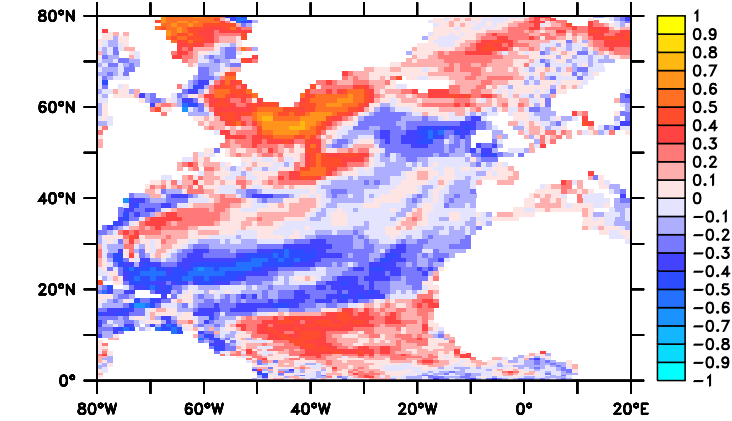

(B) $\log(H_{ML})$–AMOI Corr.: ESM2G, Aug

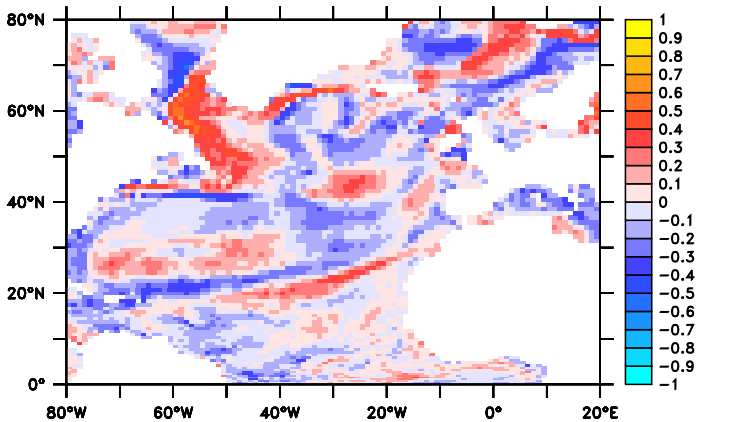

(C) $\log(H_{ML})$–AMOI Corr.: ESM2M, Mar

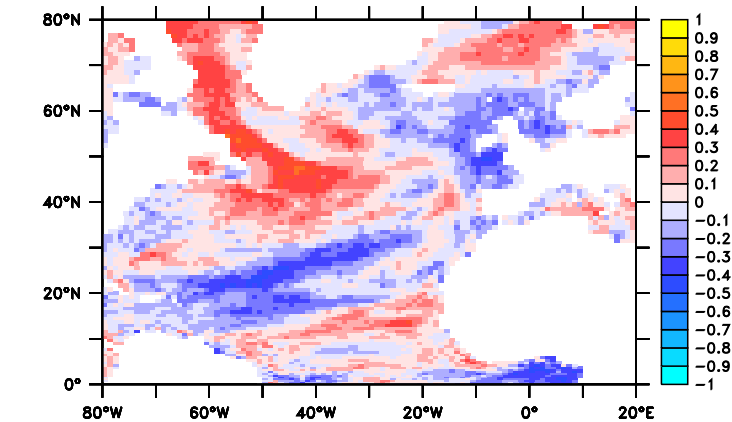

(D) $\log(H_{ML})$–AMOI Corr.: ESM2M, Aug

Figure(s)

Click here to download high resolution image

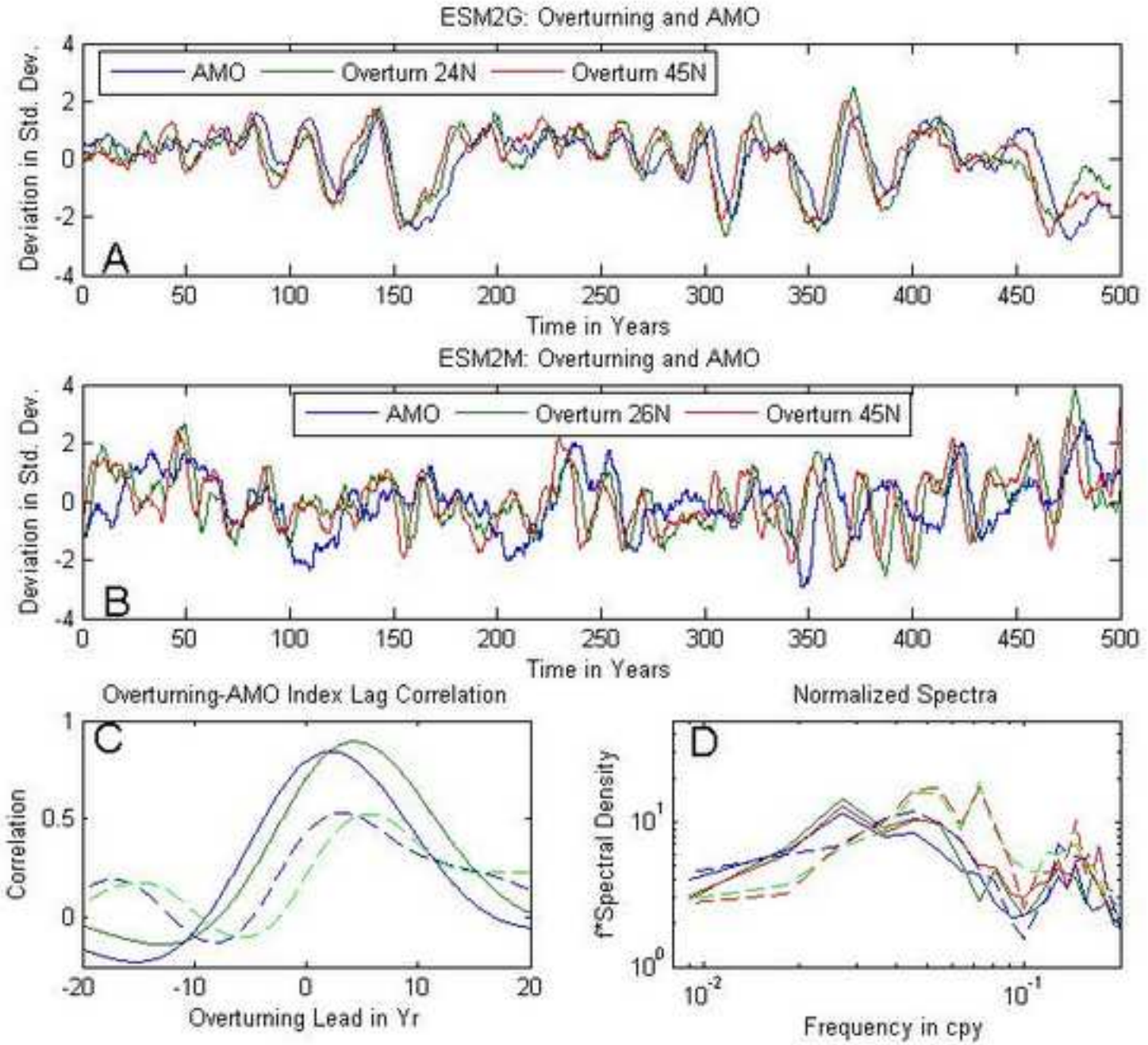

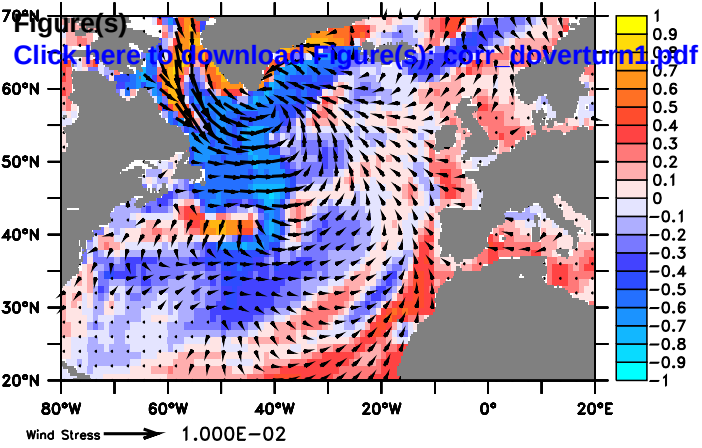

(A) PME−ψ Correlation:ESM2G

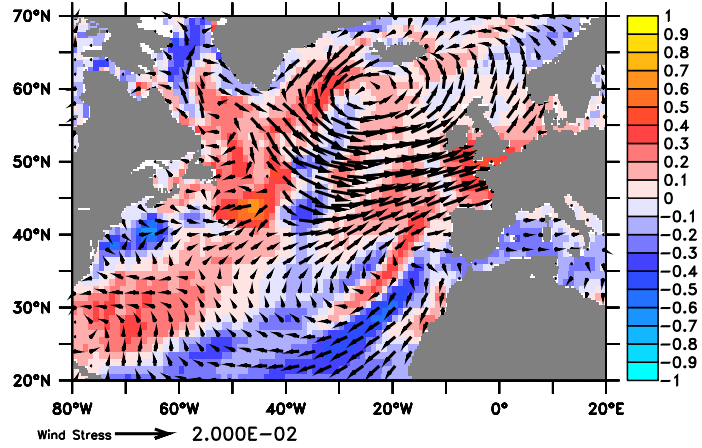

(B) PME−dψ/dt Correlation:ESM2G

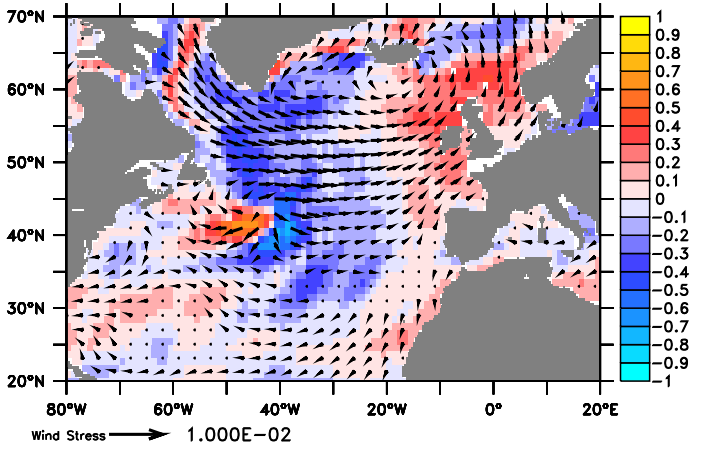

(C) PME−ψ Correlation:ESM2M

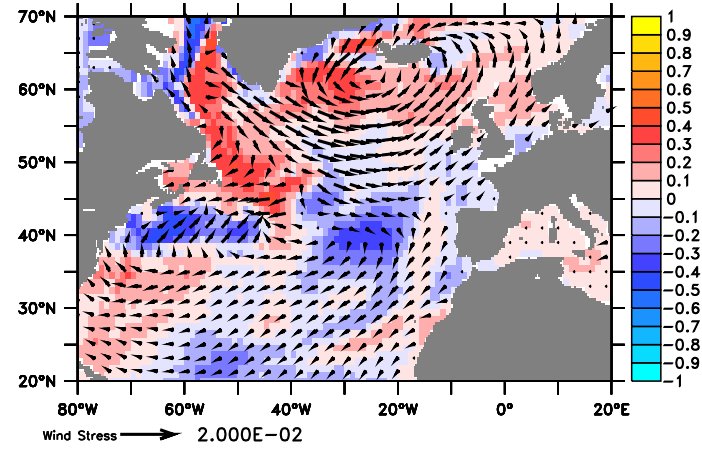

(D) PME−dψ/dt Correlation:ESM2M

Figure(s)

Click here to download Figure(s): diatom_variability.pdf

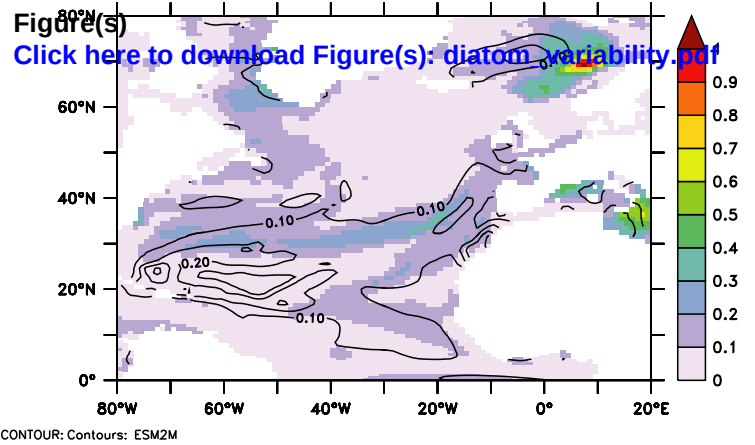

(A) COV Decadally Smoothed Diatom Biomass

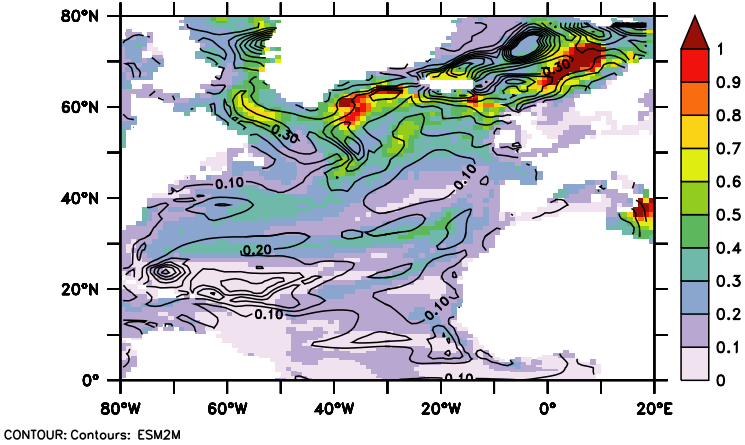

(B) COV Decadally Smoothed Apr Diatom Biomass

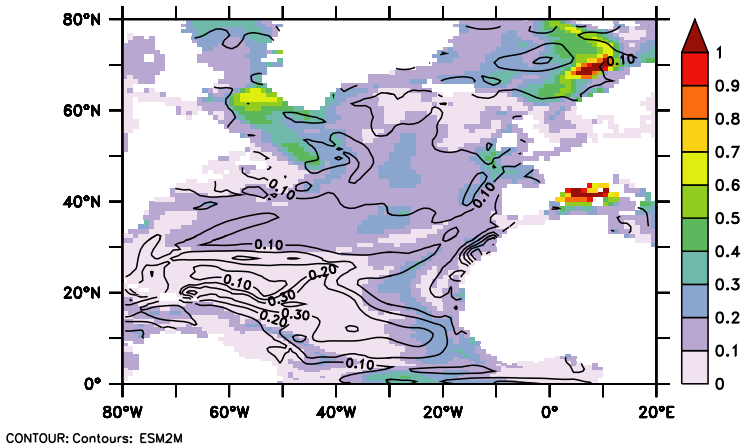

(C) COV Decadally Smoothed Jul Diatom Biomass

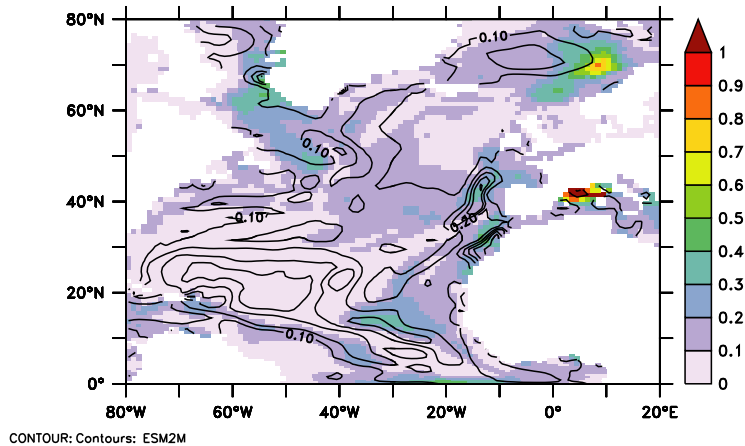

(D) COV Decadally Smoothed Oct Diatom Biomass

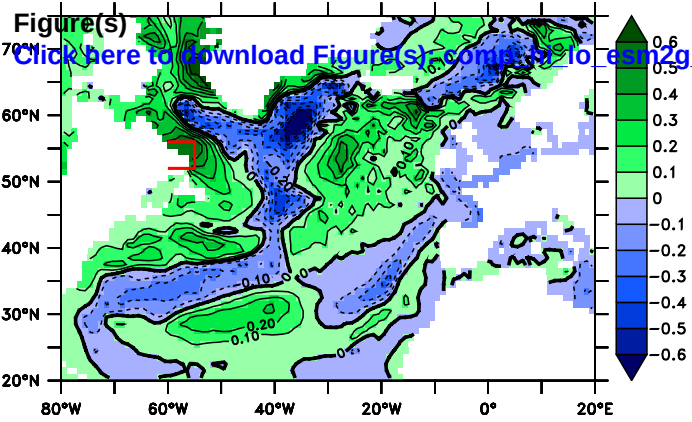

Colors: $Ln(Diat_{Hi}/Diat_{Lo})$ Contours: $NO3_{Hi}-NO3_{Lo}$

(A) Difference in Diatoms/NO_3: Apr

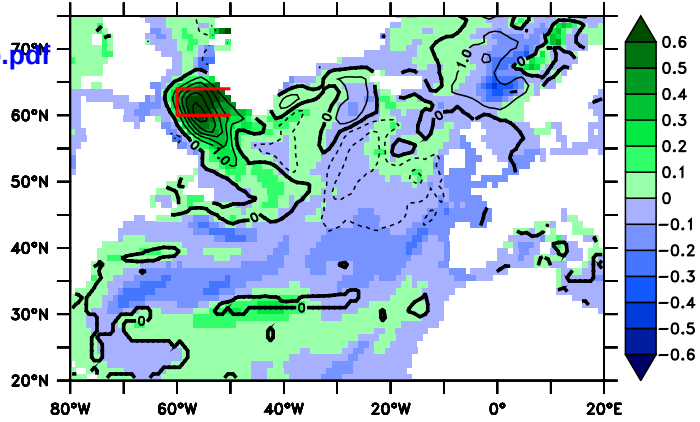

Colors: $Ln(Diat_{Hi}/Diat_{Lo})$ Contours: $NO3_{Hi}-NO3_{Lo}$

(B) Difference in Diatoms/NO_3: Jun

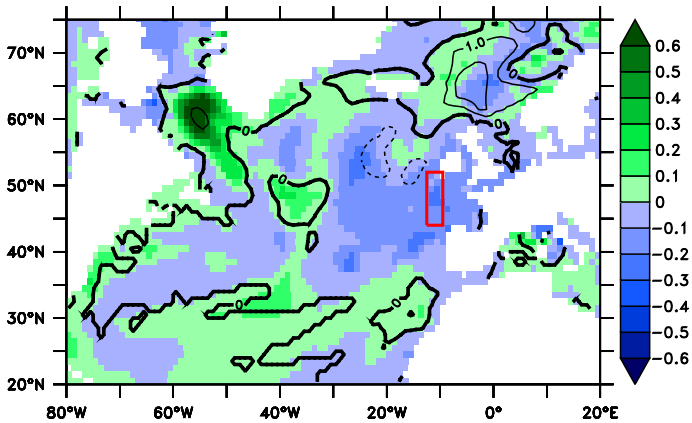

Colors: $Ln(Diat_{Hi}/Diat_{Lo})$ Contours: $NO3_{Hi}-NO3_{Lo}$

(C) Difference in Diatoms/NO_3: Aug

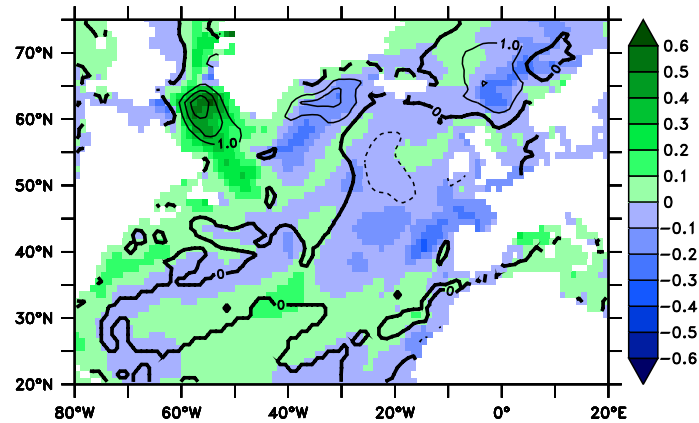

Colors: $Ln(Diat_{Hi}/Diat_{Lo})$ Contours: $NO3_{Hi}-NO3_{Lo}$

(D) Difference in Diatoms/NO_3: Oct

Figure(s)

Click here to download Figure(s): comp_hi_lo_esm2m_amo.pdf

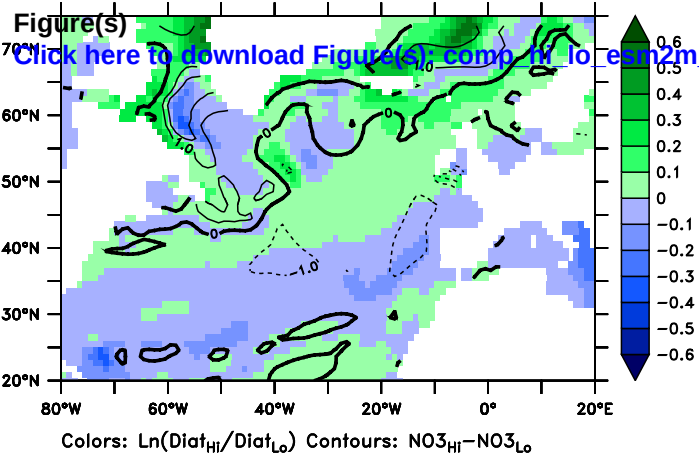

Colors: $Ln(Diat_{HI}/Diat_{Lo})$ Contours: $NO3_{HI}-NO3_{Lo}$

(A) Difference in Diatoms/NO_3: Apr

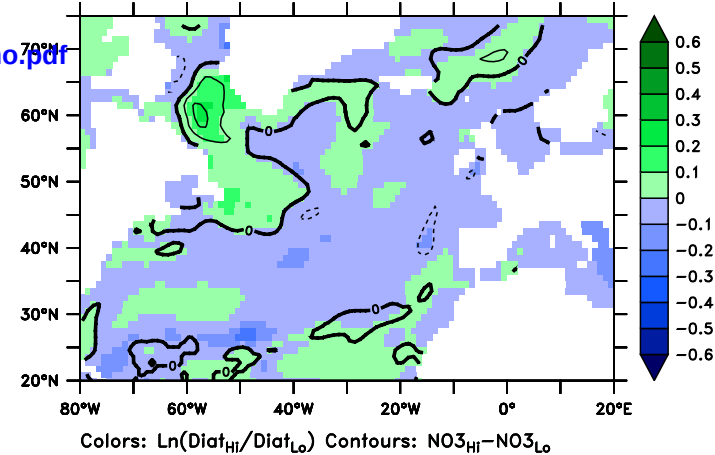

Colors: $Ln(Diat_{HI}/Diat_{Lo})$ Contours: $NO3_{HI}-NO3_{Lo}$

(B) Difference in Diatoms/NO_3: Jun

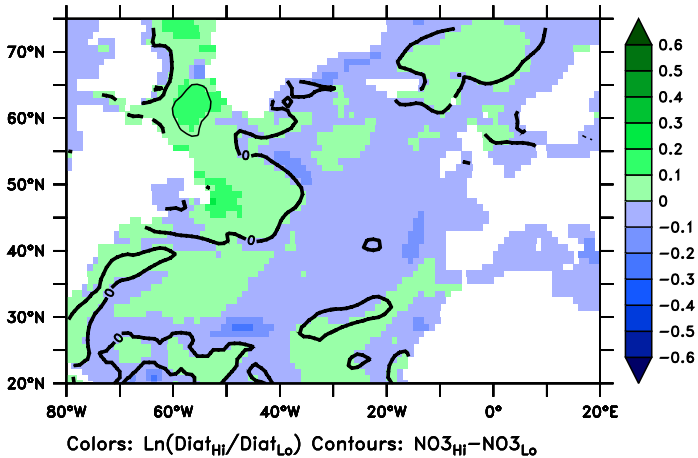

Colors: $Ln(Diat_{HI}/Diat_{Lo})$ Contours: $NO3_{HI}-NO3_{Lo}$

(C) Difference in Diatoms/NO_3: Aug

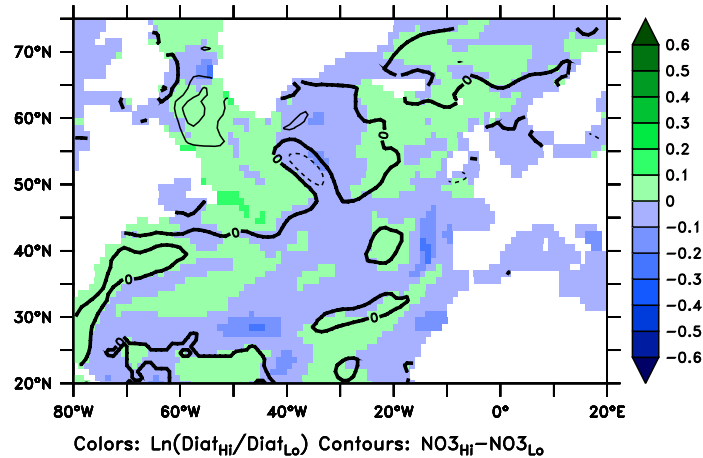

Colors: $Ln(Diat_{HI}/Diat_{Lo})$ Contours: $NO3_{HI}-NO3_{Lo}$

(D) Difference in Diatoms/NO_3: Oct

Figure(s)

Click here to download high resolution image

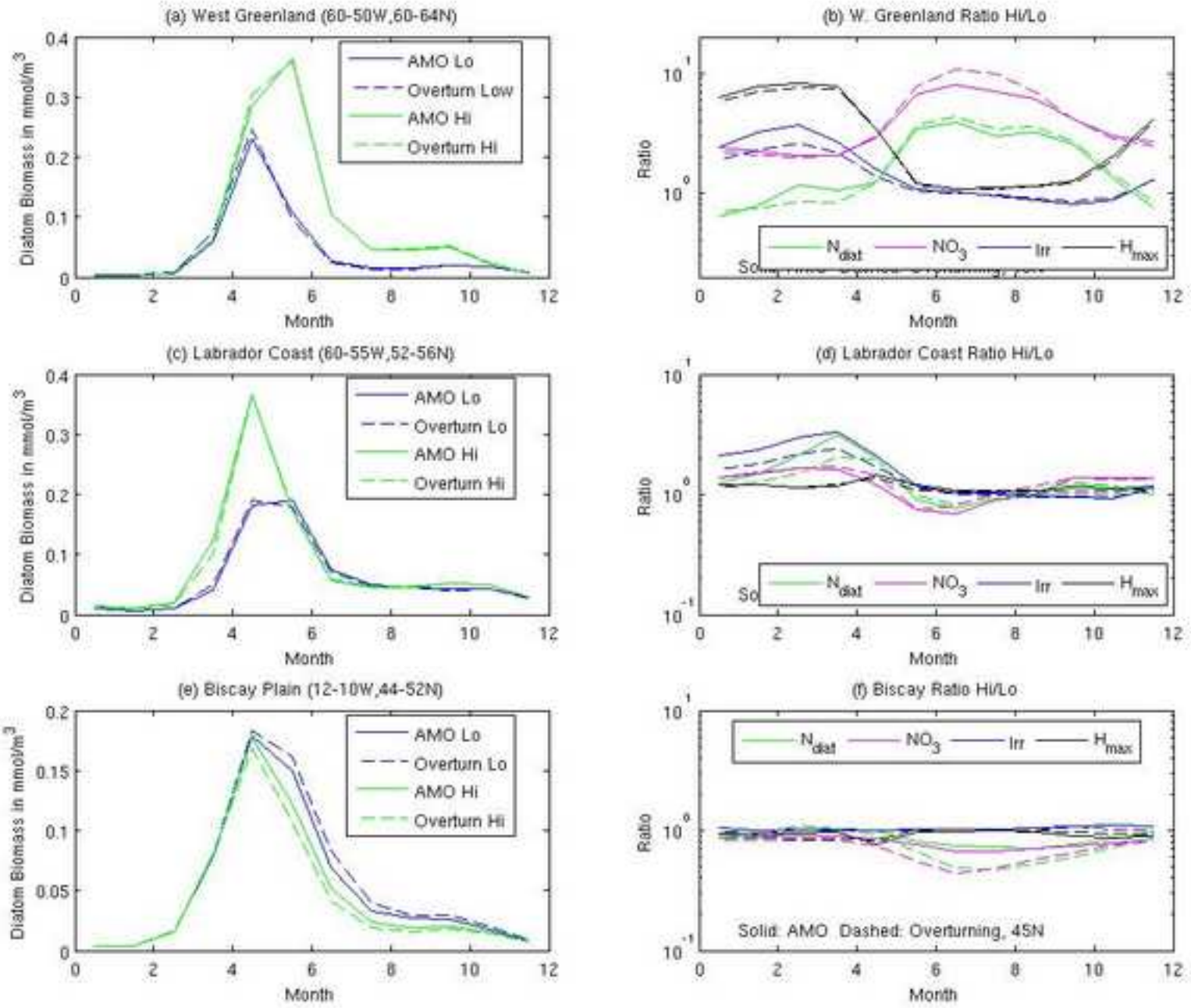

Figure(s)

Click here to download Figure(s): wgreen_analysis.pdf

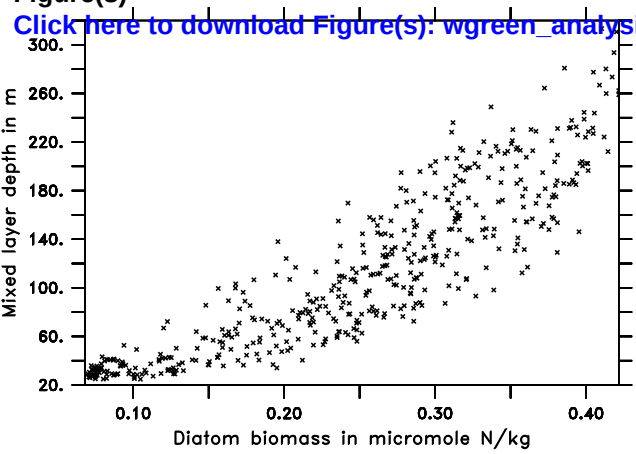

(A) Jun Diatoms vs Mar MLD, W. Greenland

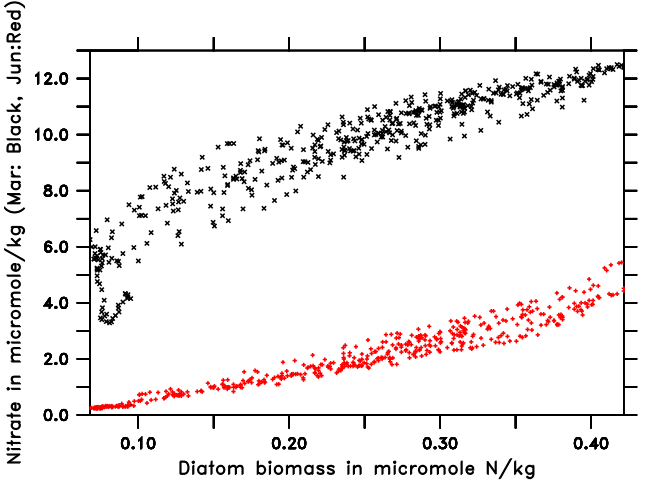

(B) Jun Diatoms vs Mar NO_3, W. Greenland

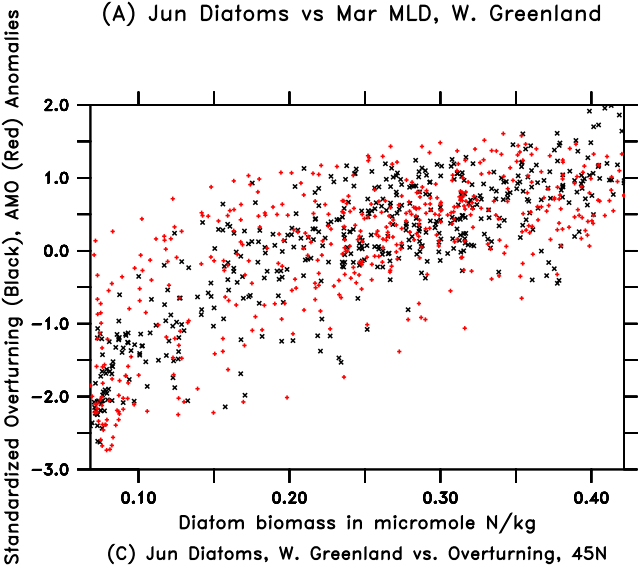

(C) Jun Diatoms, W. Greenland vs. Overturning, 45N

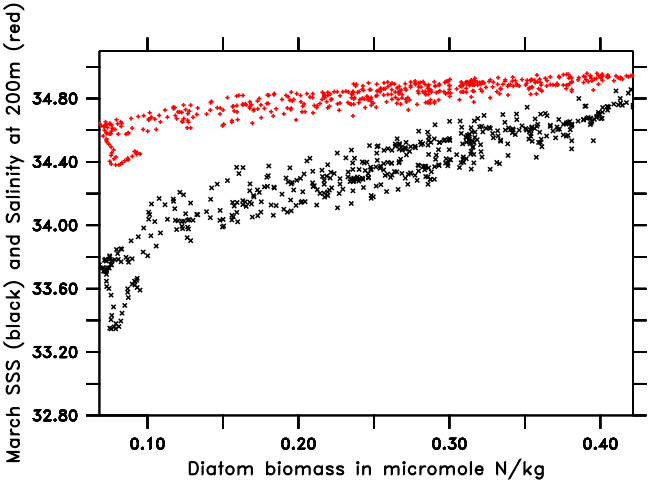

(D) Jun Diatoms vs Salinity, W. Greenland

Figure(s)

Click here to download Figure(s): labcoast_analysis.pdf

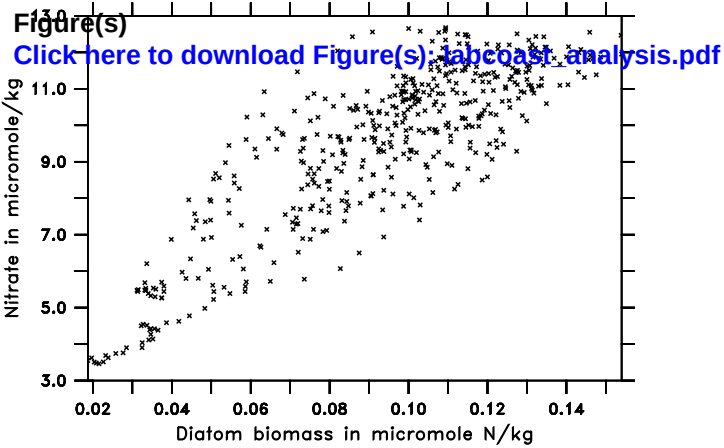

(A) Apr Diatoms vs Nitrate, Lab. Coast

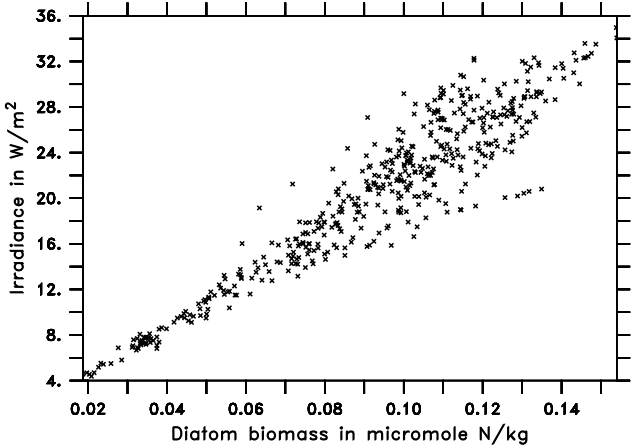

(B) Apr Diatoms vs Irradiance, Lab. Coast

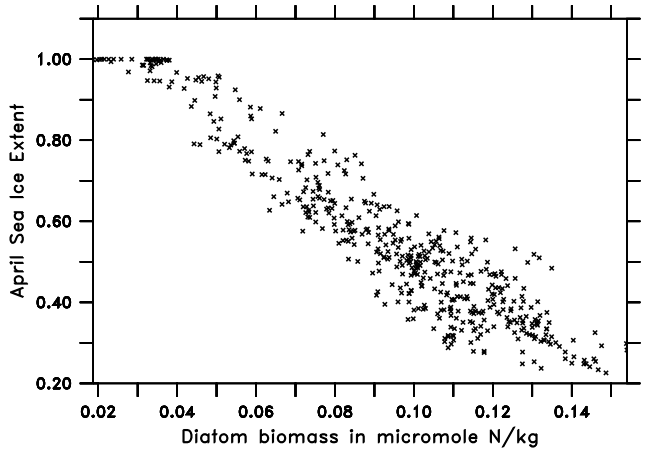

(C) Apr Diatoms vs Ice Extent, Lab. Coast

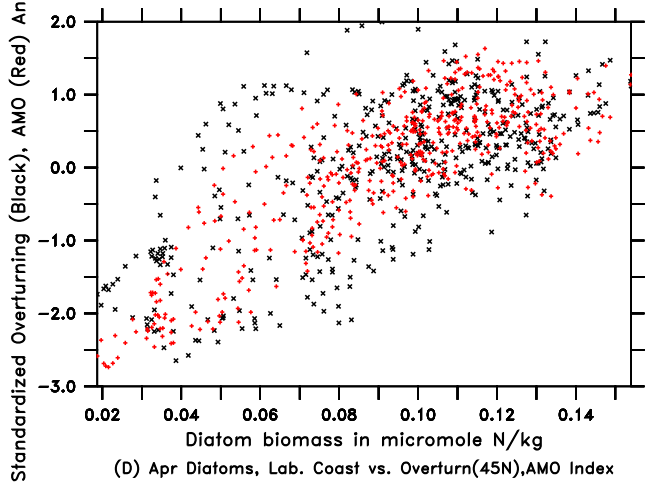

(D) Apr Diatoms, Lab. Coast vs. Overturn(45N),AMO Index

Figure(s)

Click here to download Figure(s): biscay_analysis.pdf

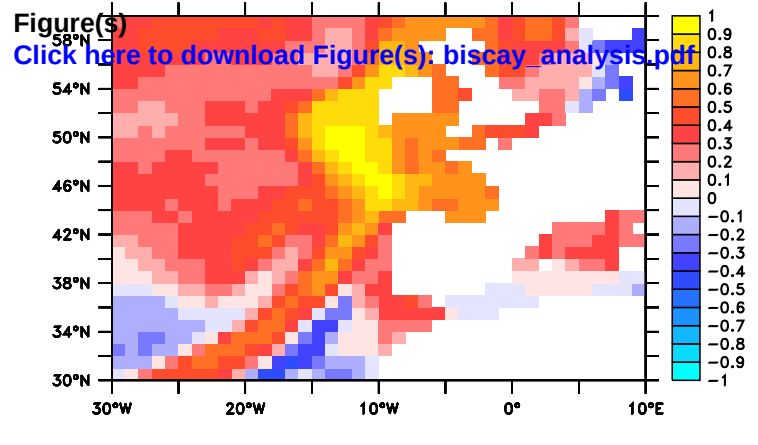

(A) Jun Biscay Diatom−Ann. Nitrate Corr.

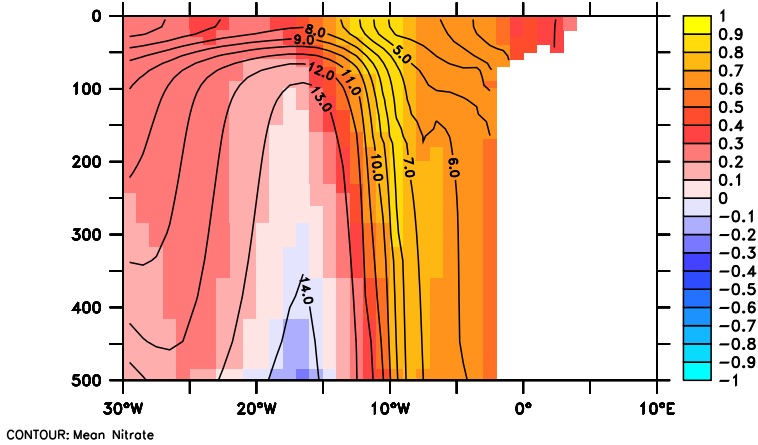

(B) Jun Biscay Diatom− Ann. Nitrate Corr.

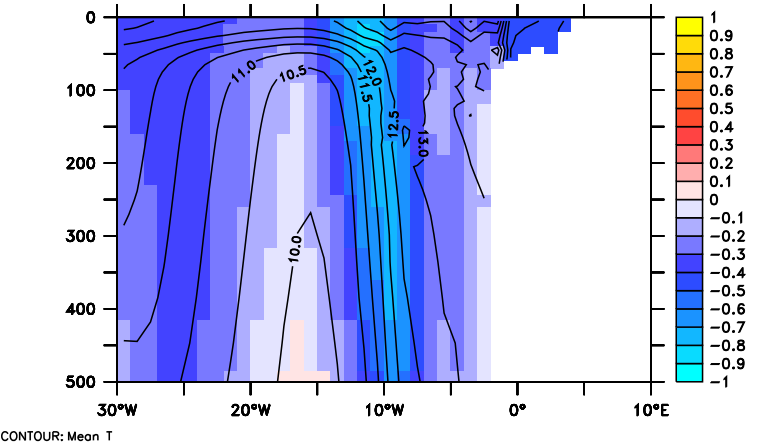

(C) Jun Biscay Diatom− Ann. Temp Corr.

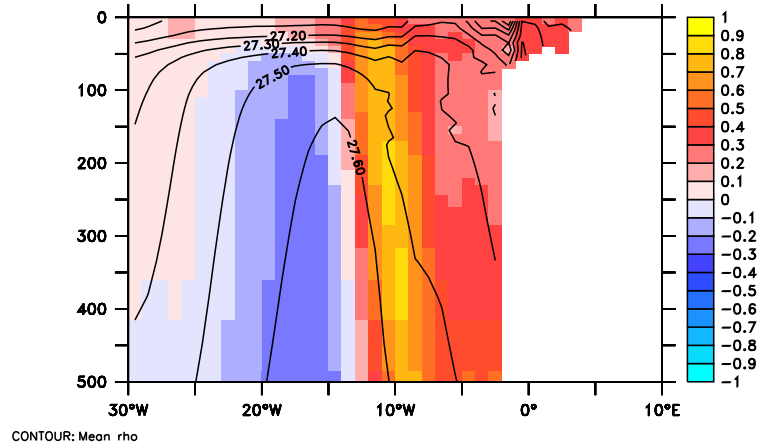

(D) Jun Biscay Diatom− Ann. Rho Corr.